A NUMERICAL AND THEORETICAL STUDY OF CERTAIN NONLINEAR WAVE PHENOMENA

By B. FORNBERG and G. B. WHITHAM, F.R.S.
Applied Mathematics, California Institute of Technology, Pasadena, California 91125, *U.S.A.*

(*Received* 30 *August* 1977)

CONTENTS

An efficient numerical method is developed for solving nonlinear wave equations typified by the Korteweg–de Vries equation and its generalizations. The method uses a pseudospectral (Fourier transform) treatment of the space dependence together with a leap-frog scheme in time. It is combined with theoretical discussions in the study of a variety of problems including solitary wave interactions, wave breaking, the resolution of initial steps and wells, and the development of nonlinear wavetrain instabilities.

1. Introduction

A number of basic equations in the study of nonlinear waves take the form

$$u_t + f(u)\, u_x + \mathscr{L} u = 0, \tag{1}$$

where $f(u)$ is a function of u and $\mathscr{L}$ is a linear operator with constant coefficients. We shall be particularly interested in the original Korteweg–de Vries equation

$$u_t + uu_x + u_{xxx} = 0, \tag{2}$$

Vol. 289. A. 1361. 32 [Published 2 May 1978

its modified forms $$u_t + (p+1)\,u^p u_x + u_{xxx} = 0, \quad p = \text{integer}, \tag{3}$$

and a generalization of the linear part leading to

$$u_t + uu_x + \int_{-\infty}^{\infty} K(x-\xi)\,u_\xi(\xi,t)\,\mathrm{d}\xi = 0, \tag{4}$$

where $K(x)$ can be chosen to give various dispersive effects. The equations

$$u_t + 3|u|^2 u_x + u_{xxx} = 0, \tag{5}$$

$$u_t + (|u|^2 u)_x + u_{xxx} = 0, \tag{6}$$

for a complex u, will also be studied briefly.

A numerical method is developed for the periodic initial value problem in which u is a prescribed function of x at $t = 0$ and the solution is periodic in x outside a basic interval $0 \leqslant x \leqslant L$. For most of the problems considered, L may be chosen large enough so the boundaries do not affect the wave interactions being studied. The method is applied in investigations of (*a*) solitary wave interactions, (*b*) wave breaking in the case of (4), (*c*) solutions for initial steps and wells in the case of the Korteweg–de Vries equation, and (*d*) the instability of finite amplitude wavetrains.

2. The numerical method

The method will be described for the Korteweg–de Vries equation (2), but can be implemented for a broad class of equations (1), with obvious changes in the various formulas. This is a Fourier or pseudospectral method (Kreiss & Oliger 1972; Fornberg 1975) in which $u(x,t)$ is transformed into Fourier space with respect to x, and derivatives (or other operators) with respect to x are algebraic in the transformed variable.

For ease of presentation the spatial period is normalized to $[0, 2\pi]$. This interval is discretized by $2N$ equidistant points, with spacing $\Delta x = \pi/N$. The function $u(x,t)$, numerically defined only on these points, can be transformed to the discrete Fourier space by

$$\hat{u}(\nu,t) = Fu = \frac{1}{\sqrt{(2N)}} \sum_{j=0}^{2N-1} u(j\Delta x, t)\,\mathrm{e}^{-\pi \mathrm{i} j\nu/N}, \tag{7}$$

$$\nu = 0, \pm 1, \ldots, \pm N.$$

The inversion formula is

$$u(j\Delta x, t) = F^{-1}\hat{u} = \frac{1}{\sqrt{(2N)}} \sum_{\nu} \hat{u}(\nu,t)\,\mathrm{e}^{\pi \mathrm{i} j\nu/N}, \tag{8}$$

where only one half of the contributions at $\nu = \pm N$ are included in the sum over ν. These transforms can be performed, efficiently with the fast Fourier transform algorithm (Cooley, Lewis & Welch 1969, 1970; Cooley & Tukey 1965).

With this scheme, u_x could be evaluated as $F^{-1}\{\mathrm{i}\nu Fu\}$, u_{xxx} as $-F^{-1}\{\mathrm{i}\nu^3 Fu\}$ and so on. Combined with a leap-frog time step, the K. de V. equation would then be approximated by

$$u(x, t+\Delta t) - u(x, t-\Delta t) + 2\mathrm{i}u\Delta t F^{-1}\{\nu Fu\} - 2\mathrm{i}\Delta t F^{-1}\{\nu^3 Fu\} = 0. \tag{9}$$

We make a modification in the last term, however, and take

$$u(x, t+\Delta t) - u(x, t-\Delta t) + 2\mathrm{i}u\Delta t F^{-1}\{\nu Fu\} - 2\mathrm{i}F^{-1}\{\sin(\nu^3\Delta t)\,Fu\} = 0. \tag{10}$$

Since $\sin(\nu^3\Delta t) = \nu^3\Delta t + O(\Delta t^3)$ the two methods are identical in the limit Δt decreasing to zero.

We describe now the idea behind (10). All consistent difference approximations to a differential equation are accurate for low enough wavenumbers but, in general, they lose accuracy rapidly for increasing wavenumbers. This applies in particular to the leap-frog time difference in (9). If we consider high wavenumbers of u in (9) the term u_{xxx} dominates uu_x. Equation (9) becomes essentially

$$u(x, t+\Delta t) - u(x, t-\Delta t) - 2\mathrm{i}\Delta t F^{-1}\{\nu^3 F u\} = 0, \tag{11}$$

as an approximation to

$$u_t + u_{xxx} = 0. \tag{12}$$

Equation (10) becomes similarly

$$u(x, t+\Delta t) - u(x, t-\Delta t) - 2\mathrm{i}F^{-1}\{\sin(\nu^3\Delta t)\, Fu\} = 0. \tag{13}$$

The fundamental difference between (11) and (13) is that equation (13) is not subject to any differencing errors. It is exactly satisfied for any solution of (12), i.e. for any ν and Δt, no matter how large. This follows from the solution of (12) for one wavenumber ν,

$$u(x, t) = \mathrm{e}^{\mathrm{i}\nu(x+\nu^2 t)},$$

which satisfies

$$u(x, t+\Delta t) = \mathrm{e}^{\mathrm{i}\nu^3\Delta t} u(x, t),$$

$$u(x, t-\Delta t) = \mathrm{e}^{-\mathrm{i}\nu^3\Delta t} u(x, t).$$

Therefore

$$u(x, t+\Delta t) - u(x, t-\Delta t) - 2\mathrm{i}\sin(\nu^3\Delta t)\, u(x, t) = 0.$$

The computational cost for (9) and (10) are in both cases three fast Fourier transforms per time step. (This increases to four if we use a conservation form with $g_x(u)$ replacing $f(u)\, u_x$ in (1).)

The next section contains an analysis of the linearized stability condition for this scheme. The accuracy of the scheme is not discussed until the last section (since the analysis depends on some theory for unstable wavetrains). Appendix B contains a discussion on nonlinear instabilities and 'aliasing errors'. It also contains, in table 3, technical data for the different computations.

The numerical calculations presented in this paper were carried out in single precision (accuracy between 6 and 7 decimal digits) on the IBM 370/158 computer at the California Institute of Technology. A real problem with 128 mesh points in the period required approximately 25 ms per time step (independent of dispersion relation).

The present calculations were intended only for graphical use. The step sizes Δt and Δx were chosen to make all errors in quantities like wave shape, speed and position safely below the level that can be measured from the diagrams. Whenever analytical solutions were available, they were used to verify this accuracy. Any arbitrarily high accuracy can be obtained by refining Δt and Δx (and changing to higher precision arithmetic). When Δt is halved, the overall error due to the time discretization can be expected to decrease by a factor of four (since the scheme is second order accurate in time). Both practical experience and the analysis in §9 show that a halving of the space step will reduce the spatial discretization error by up to several orders of magnitude. This rate of convergence is unmatched by any finite difference scheme (a collection of such schemes for the K. de V. equation is given by Vliegenthart (1971)) or split step scheme which partly relies on finite differences (Tappert 1974). A purely spectral scheme would however have a potential accuracy similar to the present method. In such schemes the differential equation is transformed to Fourier space. The components for different wavenumbers are advanced in time numerically. Simple nonlinearities like uu_x have to be handled as convolutions of Fourier components. Schamel & Elsässer (1976) compare the accuracies of one pseudospectral implementa-

tion and a spectral scheme for K. de V.-type equations. They found disastrous 'aliasing errors' in the pseudospectral scheme. Since no such errors have been observed in the present calculations, their conclusions are not relevant to our implementation.

3. Linear stability analysis of the numerical method

We consider the linear model equation

$$u_t + \alpha u_x + u_{xxx} = 0, \quad \alpha \text{ constant}, \tag{14}$$

approximated in the proposed method by

$$u(x, t+\Delta t) - u(x, t-\Delta t) + 2\mathrm{i}\alpha\Delta t F^{-1}\{\nu F u\} - 2\mathrm{i}F^{-1}\{\sin(\nu^3\Delta t)\, F u\} = 0, \tag{15}$$

and use standard Fourier analysis to determine the condition which has to be imposed on the time step Δt for stability. We look for a solution to (15) of the form

$$u(x, t) = \kappa^{t/\Delta t}\mathrm{e}^{\mathrm{i}\nu x}.$$

Substitution in (15) gives

$$\kappa^{(t+\Delta t)/\Delta t}\mathrm{e}^{\mathrm{i}\nu x} - \kappa^{(t-\Delta t)/\Delta t}\mathrm{e}^{\mathrm{i}\nu x} = 2\mathrm{i}\sin(\nu^3\Delta t)\,\kappa^{t/\Delta t}\mathrm{e}^{\mathrm{i}\nu x} - 2\mathrm{i}\nu\alpha\Delta t\kappa^{t/\Delta t}\mathrm{e}^{\mathrm{i}\nu x},$$

i.e.

$$\kappa^2 - 2\mathrm{i}f(\Delta t, \nu, \alpha)\,\kappa - 1 = 0,$$

where

$$f(\Delta t, \nu, \alpha) = \sin(\nu^3\Delta t) - \nu\alpha\Delta t.$$

The scheme is conditionally stable if and only if $f(\Delta t, \nu, \alpha)$ is real and less than one in magnitude. Let us again assume for simplicity that the period is $[0, 2\pi]$ and that this interval is discretized with $2N$ equidistant meshpoints, i.e.

$$\Delta x = \pi/N.$$

The wavenumber ν takes the values

$$\nu = 0, \pm 1, \ldots, \pm N. \tag{16}$$

We want to find the largest value of Δt such that

$$|f(\Delta t, \nu, \alpha)| < 1 \tag{17}$$

is true for all ν in (16). The most severe restriction on Δt is imposed for the ν which are largest in magnitude, i.e. for $\nu = \pm\nu_{\max}$, $\nu_{\max} = N = \pi/\Delta x$. The function

$$f(\Delta t, \nu_{\max}, \alpha) = \sin\left[\Delta t\left(\frac{\pi}{\Delta x}\right)^3\right] - \Delta t\frac{\pi}{\Delta x}\alpha$$

is rapidly oscillating as a function of Δt with maxima and minima approximately

$$1 - \Delta t_1\frac{\pi}{\Delta x}\alpha, \quad -1 - \Delta t_2\frac{\pi}{\Delta x}\alpha, \quad 1 - \Delta t_3\frac{\pi}{\Delta x}\alpha, \quad -1 - \Delta t_4\frac{\pi}{\Delta x}\alpha, \text{ etc.},$$

taken for

$$\Delta t = \Delta t_1 \approx \frac{\Delta x^3}{2\pi^2}, \quad \Delta t = \Delta t_2 \approx \frac{3\Delta x^3}{2\pi^2}, \quad \Delta t = \Delta t_3 \approx \frac{5\Delta x^3}{2\pi^2}, \quad \Delta t = \Delta t_4 \approx \frac{7\Delta x^3}{2\pi^2},$$

respectively. If α is positive the inequality (17) is valid up to the second extremum, i.e., the stability condition becomes

$$\frac{\Delta t}{\Delta x^3} < \frac{3}{2\pi^2} \approx 0.1520. \tag{18}$$

The instance of α negative would require $\Delta t/\Delta x^3 < 1/2\pi^2$ because of the first extremum, but this case can easily be circumvented. If we write (14) as

$$u_t + (c+\alpha)\, u_x + (u_{xxx} - cu_x) = 0,$$

we can choose the constant c to make $(c+\alpha)$ positive. We have only to replace α by $(c+\alpha)$ and $\sin(\nu^3\Delta t)$ by $\sin(\nu^3\Delta t - c\nu\Delta t)$ in (15) to be in the previous instance.

Stability conditions for some straightforward finite difference approximations of (14) (or (12) for Δx small) are given in table 1. Here u_t is approximated by leap-frog and u_{xxx} by compact centred approximations. The limit of finite difference methods with orders of accuracy increasing to infinity is identical to the pseudospectral method according to (9) (without the nonlinear part). Apart from this limit method, the values of the stability constants for practical methods are all of the same order of magnitude.

TABLE 1

method		stability restriction on $\Delta t/\Delta x^3$	
time	space		
$l-f$	2nd order	$2/3\sqrt{3}$	≈ 0.3849
$l-f$	4th order	$54/\sqrt{(25762+4234\sqrt{73})}$	≈ 0.2170
$l-f$	6th order	—	0.1621
$l-f$	8th order	—	0.1347
⋮	⋮		⋮
$l-f$	limit of increasing orders	$1/\pi^3$	≈ 0.0323
proposed scheme		$3/2\pi^2$	≈ 0.1520

In the last section of the paper we will analyse the accuracies of these methods as functions of Δx for a strongly nonlinear solution. We will in particular compare the proposed scheme, which formally is of infinite order of accuracy, with the difference methods of finite orders. Since the maximal time step is proportional to the cube of Δx, it is important to know how large the values of Δx may be for different levels of overall accuracy.

If the linear term is $\int K(x-\xi)\, u_\xi \,\mathrm{d}\xi$ instead of u_{xxx}, the finite difference methods are no longer applicable. The stability limit for the proposed scheme depends on the associated dispersion relation. In the case $K(x) = \frac{1}{4}\pi \mathrm{e}^{-\frac{1}{2}\pi|x|}$ the condition is of the form $\Delta t/\Delta x <$ constant.

4. SOLITARY WAVE INTERACTIONS

We first use the numerical method to study the interaction of solitary waves for the equations noted in § 1. For the original K. de V. equation (2), the solitary wave solution is

$$u = 3\alpha^2 \operatorname{sech}^2 \tfrac{1}{2}(\alpha x - \alpha^3 t), \tag{19}$$

where the parameter α determines both the amplitude and speed. In the modified form (3), the corresponding solution has

$$u^p = \tfrac{1}{2}(p+2)\, \alpha^2 \operatorname{sech}^2 \tfrac{1}{2}p(\alpha x - \alpha^3 t). \tag{20}$$

(For $p = 1$, there is a different normalization factor of 2 between (2) and (3), and between (19) and (20).) When p is odd, (20) is a positive wave with $u \geqslant 0$; if the sign of the nonlinear term in (3) is changed, there is a change of sign in (20) and the solitary wave has $u \leqslant 0$. When p is even, either sign may be taken for u in (20); there are no solitary wave solutions, when p is even, if the sign of the nonlinear term is changed in (3).

Figures 1–6 show typical interactions for the original K. de V. equation and its modified forms with $p = 2, 3, 4$. For the K. de V. equation, an explicit analytic formula was given by Gardner, Greene, Kruskal & Miura (1967, 1974) for the interaction of N unequal solitary waves. If the parameters are $\alpha_1, \alpha_2, \ldots, \alpha_N$, it may be written

$$u = 12\partial^2 \ln |D|/\partial x^2, \tag{21}$$

where $|D|$ is the determinant with elements

$$D_{mn} = \delta_{mn} + \frac{2}{\alpha_m + \alpha_n} e^{-\alpha_m(x-x_m)+\alpha_m^2 t}, \tag{22}$$

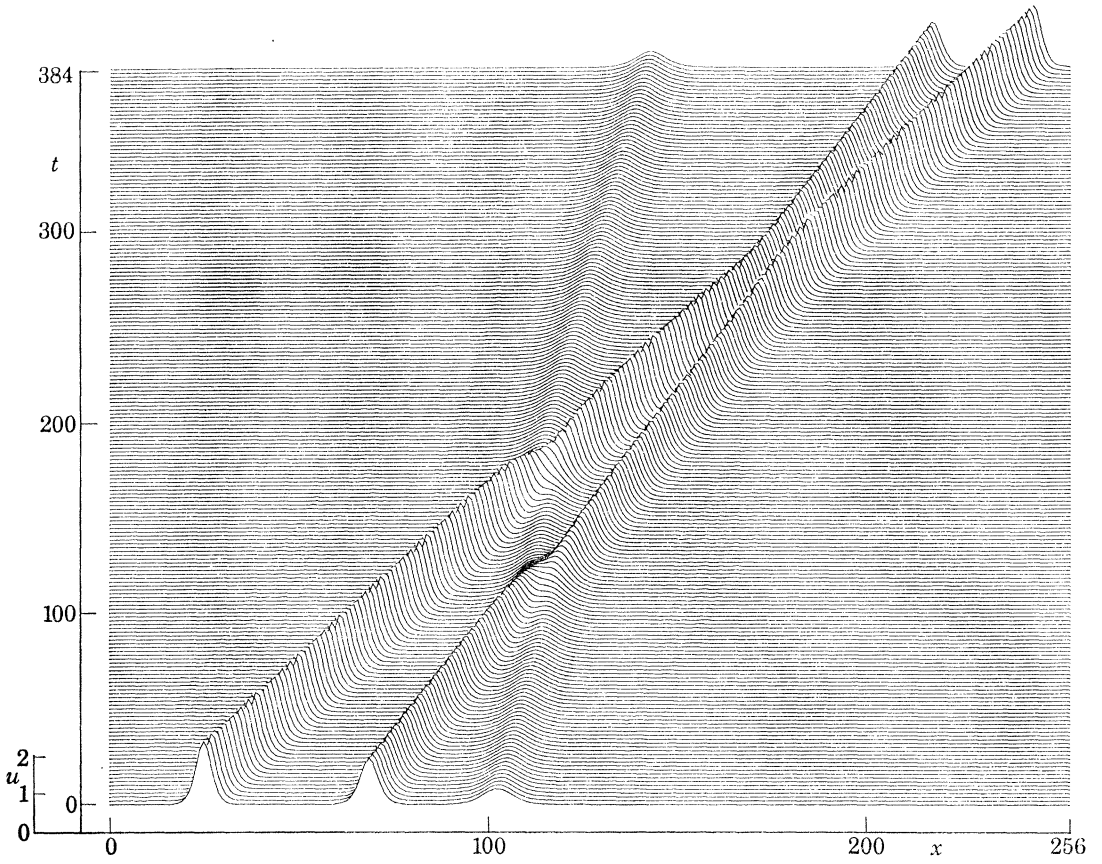

FIGURE 1. Solitary wave interaction for $u_t + uu_x + u_{xxx} = 0$.

the subsidiary parameters x_m controlling the initial separation of the waves. A similar formula is available in the case $p = 2$. From these formulas it can be deduced that the solitary waves eventually emerge unchanged, the only memory of the interaction being a constant displacement of the position from the path each one would have otherwise followed. For the interaction of two waves with parameters $\alpha_2 > \alpha_1$, the stronger wave has a forward shift and the weaker wave a backward shift, given respectively by

$$\frac{1}{\alpha_2} \ln \left(\frac{\alpha_2 + \alpha_1}{\alpha_2 - \alpha_1} \right)^2, \quad \frac{1}{\alpha_1} \ln \left(\frac{\alpha_2 + \alpha_1}{\alpha_2 - \alpha_1} \right)^2. \tag{23}$$

These formulas apply to both cases $p = 1$ and $p = 2$.

This 'clean interaction' of solitary waves is seen in figures 1–3. For the K. de V. solution (21), it has been shown by Lax (1968) that the character of the interaction between any pair of solitary waves changes according as the ratio of their speeds is below, between, or above the critical values

$$\tfrac{1}{2}(3+\sqrt{5}) = 2.618 \quad \text{and} \quad 3.$$

In the calculations of figure 1, the speeds were chosen to be

$$\alpha_1^2 = 0.55, \quad \alpha_2^2 = 0.40, \quad \alpha_3^2 = 0.14,$$

so that

$$\alpha_1^2/\alpha_2^2 = 1.375 < 2.618 < \alpha_2^2/\alpha_3^2 = 2.857 < 3 < \alpha_1^2/\alpha_3^2 = 3.929,$$

and all three cases were included. For the (1, 2) interaction, with speed ratio below the lower critical, there are always two maxima; the waves approach each other and exchange rôles, but then shear away and do not pass through each other. In the (1, 3) and (2, 3) interactions the waves pass through each other and in each case the smaller maximum disappears during this process. For the (1, 3) interaction, with speed ratio above the upper critical, the larger maximum just decreases to a certain least value at time $t = T$ then increases again. At time $t = T$ there is just a single maximum; the interaction is symmetric in time about $t = T$. For the (2, 3) interaction with speed ratio between the critical values, the larger maximum decreases and disappears, but before this happens a new maximum replacing it has appeared at a displaced position and takes over its rôle. At the point of symmetry in time there are two equal maxima. This however can not be seen clearly in figure 1.

For the modified equation with $p = 2$, the interaction of the two positive solitary waves shown in figure 2 appears as close approach and interchange of rôles, whereas for the positive and negative waves in figure 3 the impression is one of the waves crossing. For two positive waves, the stronger wave weakens during the interaction and then recovers. During the interaction with a negative wave, a stronger positive wave increases in height and narrows. The smaller wave disappears on its front and is recreated at the back.

For the modified forms with $p \geqslant 3$, exact solutions for interactions are not known and it is believed that this goes along with essential differences in the behaviour. The methods of finding solutions such as (21) (inverse scattering, Bäcklund transformations, etc.) are remarkably ingenious and the fact alone that solutions have not been found in any particular case would leave the question open. However, these methods also seem to be closely tied to the existence of an infinite number of conservation laws of the form

$$\frac{\partial}{\partial t}P\{u\} + \frac{\partial}{\partial x}Q\{u\} = 0,$$

and corresponding integrals

$$\int_{-\infty}^{\infty} P\{u\}\,\mathrm{d}x = \text{constant},$$

if convergent, where P and Q are functions u and its derivatives. It is often possible to make progress on the existence of conservation laws and then infer the possibility of related methods of solution. Since the clean interaction of solitary waves was first shown from the explicit solutions and had previously been considered unlikely, it has also been conjectured that equations with an appropriate infinity of conservation laws will show clean interactions and those without will not. The direct connection appears to be the intuitive idea that the infinite number of integrals forces conservation of the identities of the waves.

In some of the cases for which exact solutions are known by inverse scattering techniques, the existence of conservation laws and clean interactions can be related to the fact that the equations can be cast as a completely integrable Hamiltonian system (Zhakarov & Shabat 1972). The latter appears to be another general way of distinguishing these cases. The conserved integrals mentioned above become action variables for the system.

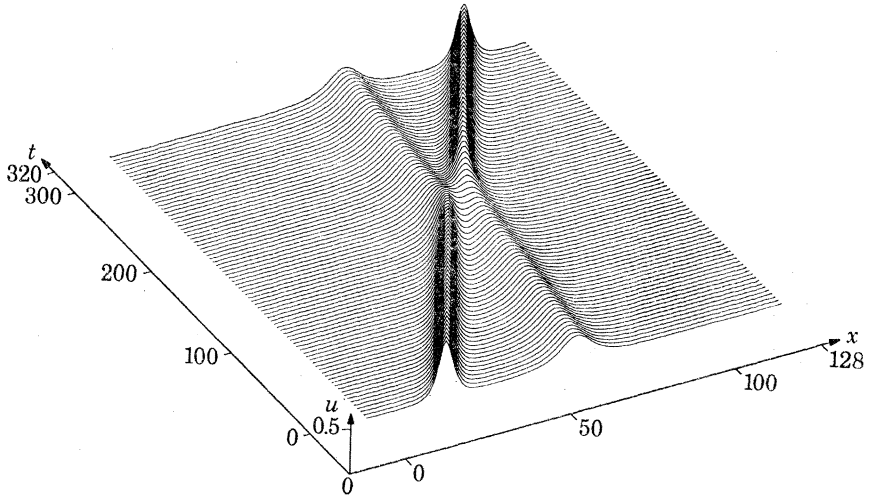

FIGURE 2. Solitary wave interaction for $u_t+3u^2u_x+u_{xxx}=0$.

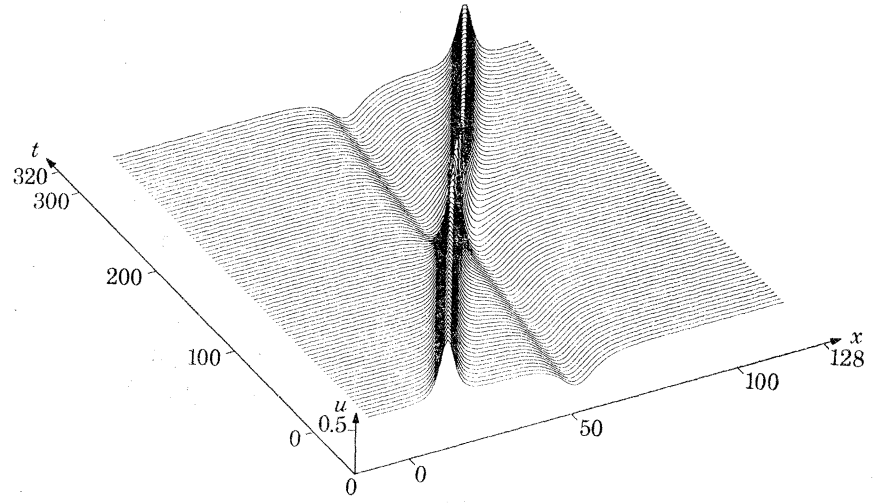

FIGURE 3. Solitary wave interaction for $u_t+3u^2u_x+u_{xxx}=0$.

For the modified K. de V. equation, it is known that there are an infinite number of conservation laws when $p=1$ and 2, but not when $p\geqslant 3$. According to the conjecture, then, interactions should no longer be clean when $p\geqslant 3$. Figures 4 and 5 show numerical results for $p=3$. There are small but definite disturbances behind the second wave after the interaction that are too large to be numerical errors. For the case $p=4$, shown in figure 6, the development of an additional disturbance is more obvious, and we easily conclude that the interaction is not clean. The calculations were not run for the very long times that would be required to resolve the interesting question of whether the extra disturbance develops into a further solitary wave or is a tail that dies out asymptotically as $t\to\infty$.

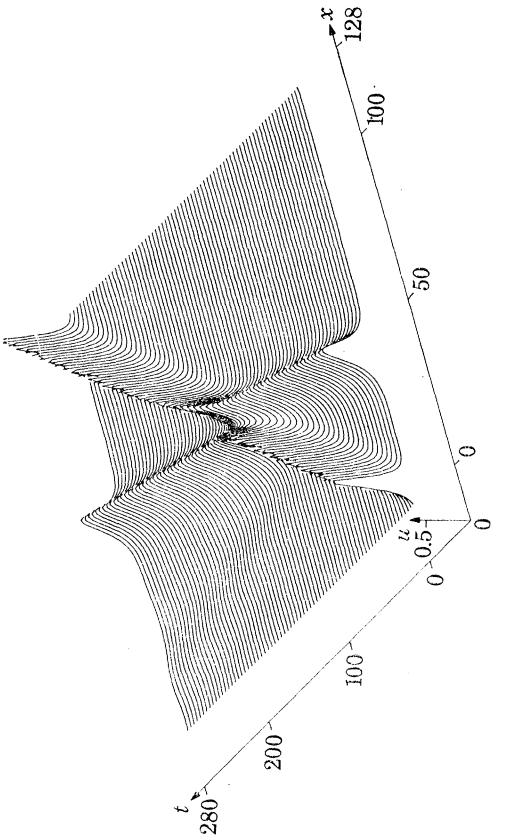

FIGURE 5. Solitary wave interaction for $u_t + 4u^3u_x + u_{xxx} = 0$.

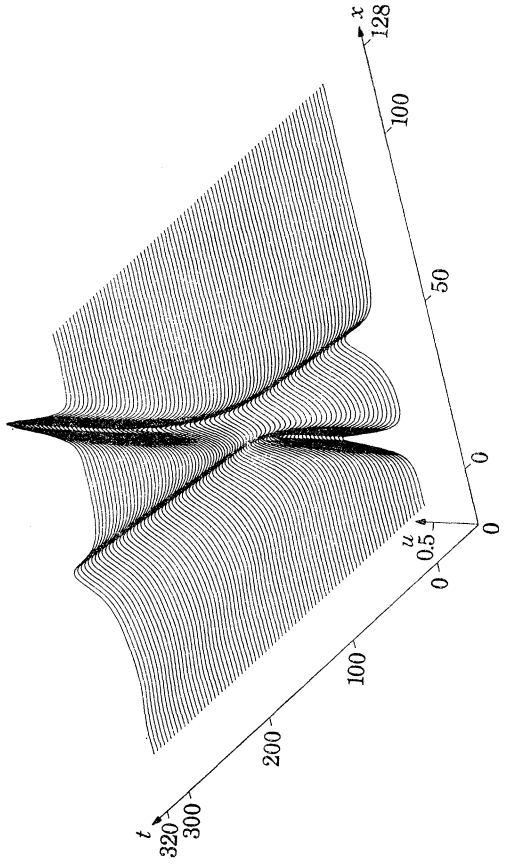

FIGURE 4. Solitary wave interaction for $u_t + 4u^3u_x + u_{xxx} = 0$.

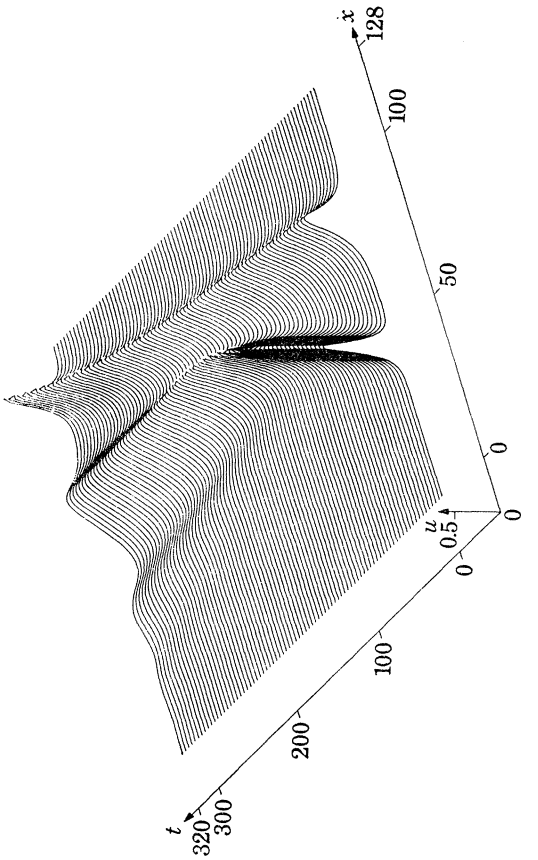

FIGURE 6. Solitary wave interaction for $u_t + 5u^4u_x + u_{xxx} = 0$.

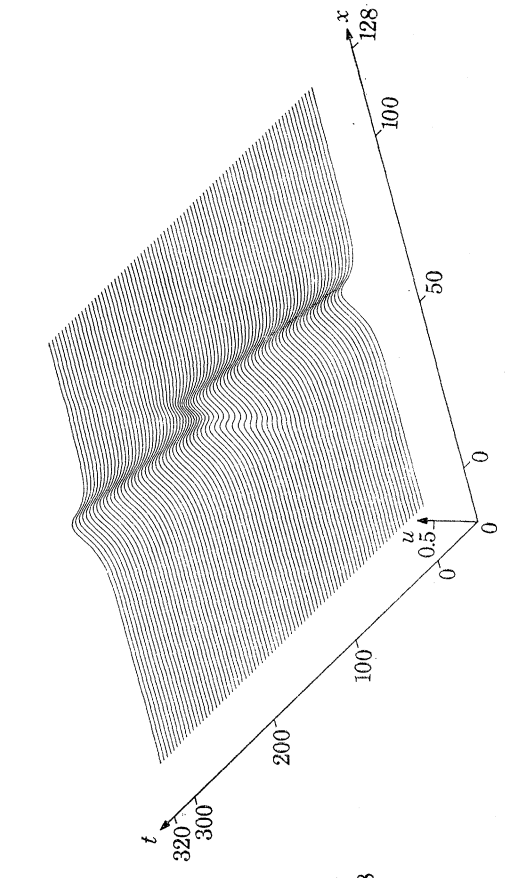

FIGURE 8. Imaginary part corresponding to figure 7.

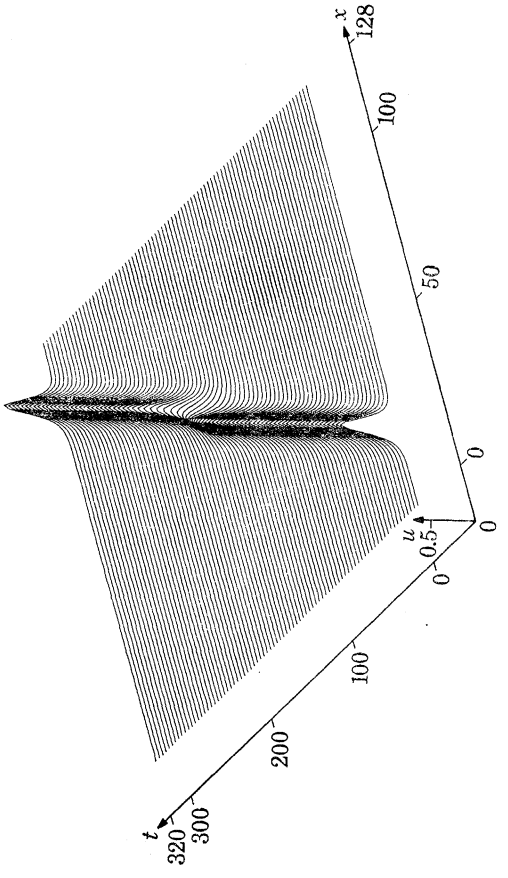

FIGURE 7. Solitary wave interaction for $u_t + 3|u|^2 u_x + u_{xxx} = 0$: real part.

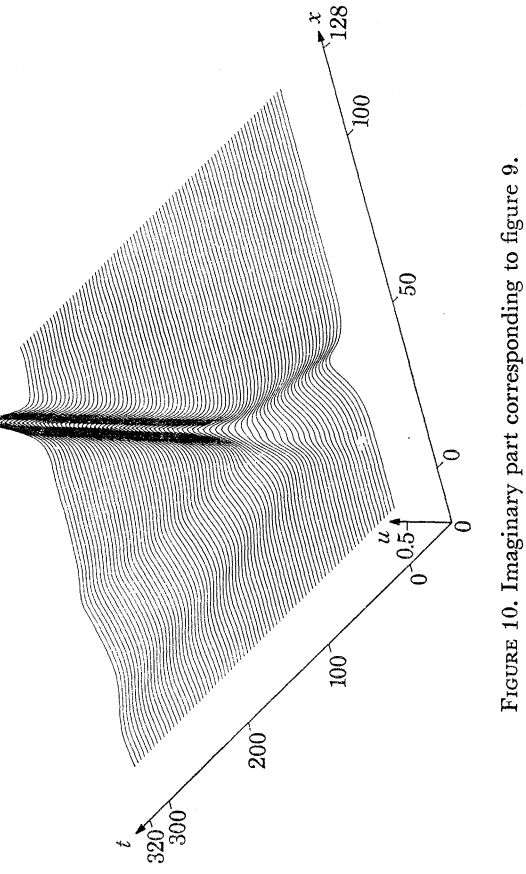

FIGURE 10. Imaginary part corresponding to figure 9.

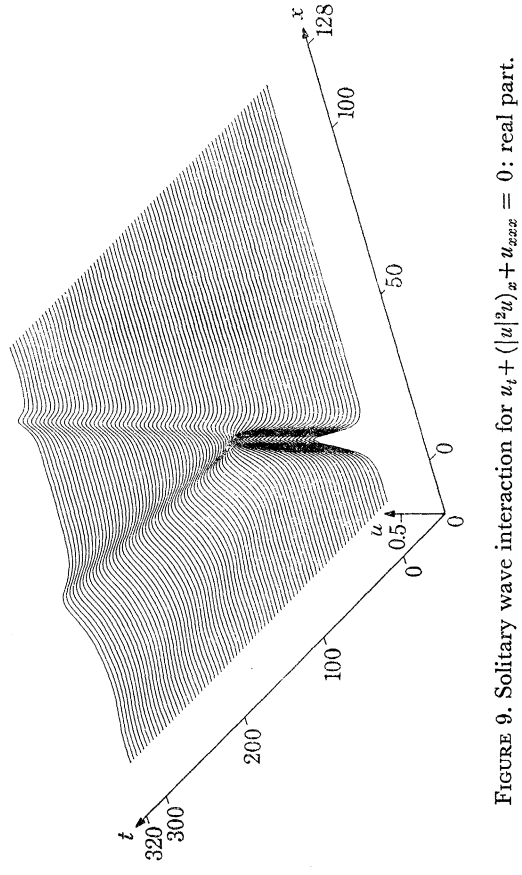

FIGURE 9. Solitary wave interaction for $u_t + (|u|^2 u)_x + u_{xxx} = 0$: real part.

Of course, although the interactions for $p = 3$ and $p = 4$ are not precisely clean, there is a considerable preservation of the original waves and the usual interchange of rôles.

Figure 7–10 show interactions for the equations (5) and (6) with u complex. If any real solution (20), with $p = 2$ is multiplied by a complex number with modulus one, we obtain a complex solitary wave for (5) or (6). The figures show the interaction of a purely real and a purely imaginary wave. For equation (5), the real part is shown in figure 7 and the imaginary part in figure 8. The interaction is seen to be clean with the usual displacement in position. For equation (6), figures 9 and 10 show the real and imaginary parts, respectively. In this case, it is seen that there is considerable new disturbance introduced into the real part along the path of the imaginary part and vice versa. There is also a tail following the slower wave after the interaction. These results again fit the various conjectures, since (5) is known to have the required conservation laws, inverse scattering applies, etc., whereas (6) is thought not to have these properties.

As a possible counter to the conjecture about clean interactions, Dodd & Bullough (1976, 1977) have shown that the double Sine–Gordon equation

$$z_{xx} - z_{tt} = \lambda_1 \sin \tfrac{1}{2}z + \lambda_2 \sin z$$

has neither an infinite number of conservation laws nor Bäcklund transformations, yet their calculations of solitary waves appeared to show clean interactions.

In our computations on the integro-differential equation (4), described in § 6, we also find clean interactions and do not at present expect there to be appropriate conservation laws, etc. Before describing these results, we note briefly some further computations for the modified K. de V. equation with $p = 2$.

5. Wave packets

For some equations there are solutions closely related to the ordinary solitary waves which are oscillatory disturbances inside a wave envelope, where the envelope has a solitary wave appearance. They have been variously referred to as wave packets, envelope solitons or breathers.

In the case of the complex equation

$$u_t + 3|u|^2 u_x + u_{xxx} = 0,$$

these solutions can be found directly by elementary means and take the form

$$u = \sqrt{2}\ \alpha \operatorname{sech}(\alpha x - \beta t)\, e^{i(kx - \omega t)},$$

where

$$\omega/k = -k^2 + 3\alpha^2, \tag{24}$$

$$\beta/\alpha = -3k^2 + \alpha^2. \tag{25}$$

The latter two relations are interpreted as the nonlinear phase velocity and group velocity, respectively. With appropriate initial conditions, this solution was calculated numerically from the differential equation. The real part of u is shown in figure 11 for the parameter values $k = \frac{1}{5}\pi$ and $\alpha = 0.5$.

For real u, the corresponding solutions of

$$u_t + 3u^2 u_x + u_{xxx} = 0,$$

are much more involved. The solution shown in figure 12 was found numerically by taking a reasonable type of initial disturbance and adjusting it until the appropriate solution was obtained.

However, an explicit formula can be extracted from the inverse scattering or Hirota's work (Hirota 1972); it is

$$u = 2\sqrt{2}\frac{\partial}{\partial x}\arctan\left\{\frac{\alpha}{k}\operatorname{sech}(\alpha x - \beta t)\sin(kx - \omega t)\right\},$$

where the parameters satisfy the same relations as in (24), (25). Even the direct verification of this formula would be laborious, and certainly the more powerful methods were needed for its discovery. From the numerical results shown in figure 12, we estimate from the maximum height and the group speed that

$$\alpha = 0.27, \quad \beta = 0.0067.$$

From the relations in (24) and (25), we deduce that

$$k = 0.13, \quad \omega = 0.026.$$

These predictions fitted well with an independent check on the phase speed.

Since the exact solutions are known, the numerical results really provide only a check on the numerical method. But the plots give a more vivid picture of the solution.

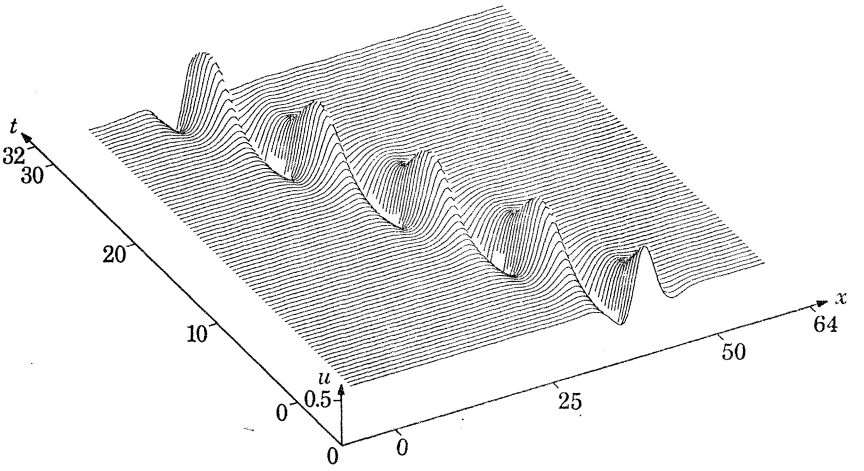

FIGURE 11. Real part of complex wave packet for $u_t + 3|u|^2 u_x + u_{xxx} = 0$.

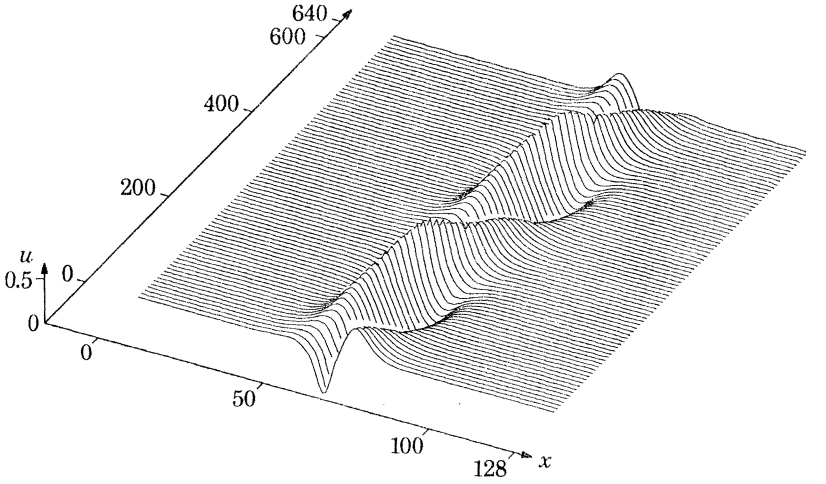

FIGURE 12. Real wave packet for $u_t + 3u^2 u_x + u_{xxx} = 0$.

6. The integro-differential equation

The Korteweg–de Vries equation was originally proposed in the context of water waves. While it is successful in predicting the existence of the observed solitary waves, it does not lead to a wave of greatest height with a peaked crest or to the other breaking phenomena of water waves. This is not surprising since it is based on long wave approximations and may be quite poor for short wave phenomena. To retain the valuable long wave behaviour but soften the third derivative term for short waves and breaking, the integral term in (4) was proposed (Whitham 1967, 1974 §13.14). The motivation is explained in detail in the original references. The aim was to find an approximate simple model to discuss some of the qualitative issues of breaking, stimulated by but not restricted to water waves. (For recent work on the full equations of water waves, see Longuet-Higgins (1976).)

The kernel $K(x)$ can be chosen to give any required linear dispersion relarion $\omega(k)$, by taking it to be the Fourier transform of the phase velocity $c(k) = \omega(k)/k$. The K. de V. equation (with an additional term u_x, normalized out in (2)) is recovered from

$$c(k) = 1-k^2, \quad K(x) = \delta(x) + \delta''(x). \tag{26}$$

The choice

$$c(k) = \nu^2/(\nu^2+k^2), \quad K(x) = \tfrac{1}{2}\nu e^{-\nu|x|}, \tag{27}$$

where ν is an adjustable parameter, is of particular interest, since it has some of the desirable features, and allows certain explicit analytic solutions to be found. For $\nu = 1$, the first two terms in the long wave expansion of $c(k)$ for small k agrees with (26). For $\nu = \frac{1}{2}\pi$, the exponential behaviour of $K(x)$ as $x \to \infty$ is closer to that of water waves. One simplifying feature of (27) is that $K(x)$ is the Green function for the operator

$$\partial^2/\partial x^2 - \nu^2, \tag{28}$$

and the equation can be reduced again to a differential equation. In the water wave context we have worked with a normalized form with a factor $\frac{3}{2}$ in front of the uu_x term in (4) and our results are quoted with that choice. The reduced differential equation for (27), with (28), is then

$$(\partial^2/\partial x^2 - \nu^2)\,(u_t + \tfrac{3}{2}uu_x) + u_x = 0. \tag{29}$$

This equation has solitary wave solutions, found as usual by taking u to be a function of $\alpha x - \beta t$ and integrating the resulting ordinary differential equation. The solution may be written

$$e^{-\alpha x+\beta t} = \frac{1-Cz}{1+Cz}\left(\frac{1+z}{1-z}\right)^{2\alpha/\nu}, \quad z = \left(\frac{a-u}{b-u}\right)^{\frac{1}{2}}, \tag{30}$$

where

$$\alpha = \frac{\nu}{2}\left(\frac{1-\frac{1}{4}m^2}{1-m^2}\right)^{\frac{1}{2}}, \quad \beta = \frac{\nu^2\alpha}{\nu^2-\alpha^2},$$

$$a = \tfrac{8}{9}(1+\tfrac{1}{2}m)\,(1-m), \quad b = \tfrac{8}{9}(1-\tfrac{1}{2}m)\,(1+m), \quad C = (b/a)^{\frac{1}{2}},$$

and m is an arbitrary parameter in the range $0 \leqslant m \leqslant 1$. The solution has $u \to 0$ as $|x| \to \infty$, and an amplitude $u = a$ at $x = 0$. As m decreases from 1 to 0, the amplitude a increases from 0 to $\frac{8}{9}$. The velocity β/α increases from 1 to $\frac{4}{3}$. For this equation there is indeed a wave of greatest height with a sharp corner at the crest. It is given by the limit $m \to 0$, and in this limit the solution simplifies down to just

$$u = \tfrac{8}{9}e^{-\frac{1}{2}\nu|x-\frac{4}{3}t|}. \tag{31}$$

In the numerical work we first considered the interaction of these solitary waves and were particularly interested to see what would happen to the wave of limiting height; a preliminary thought was that any interaction might make it break in some way. However, the result is as shown in figure 13, where the limiting wave overtakes one of smaller amplitude. There is the interchange of identities without the waves passing through each other, and as far as we can see the interaction is clean. This calculation and the perfect emergence of the peaked wave was taken to be a sensitive test of the numerical method.

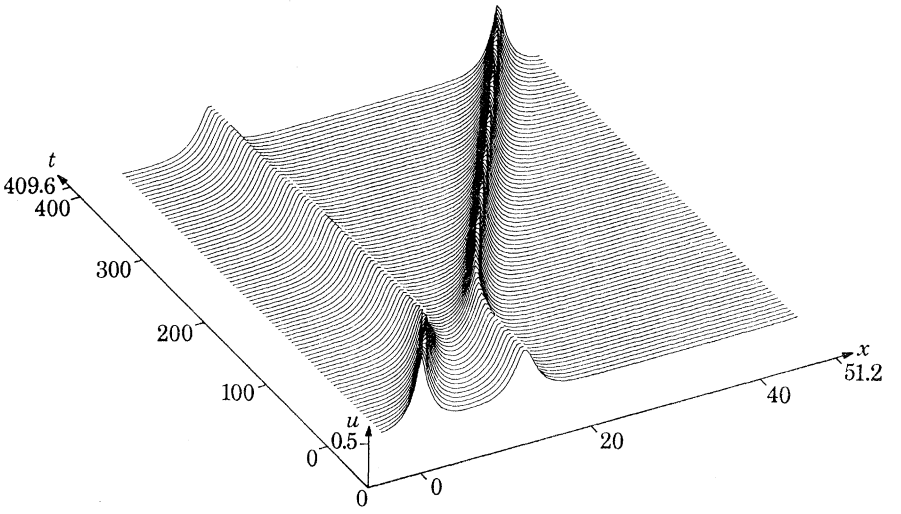

FIGURE 13. Solitary wave interaction for integral equation
$u_t+\frac{3}{2}uu_x-\frac{5}{4}u_x+\int K(x-\xi)u_\xi \mathrm{d}\xi = 0, \quad K(x) = \frac{1}{2}\nu \mathrm{e}^{-\nu|x|}, \quad \nu = \frac{1}{2}\pi.$

In view of the complicated form of the solitary wave (30) in this case, it seems unlikely that analytic formulas will be found. In all the known cases the interaction formulas express some transformed variables as sums of exponentials. The right hand side of (30) might appear to be such a transformation, but it involves the parameters of the particular solitary wave in a non-trivial way. It is different for each solitary wave so it is hard to see any kind of superposition.

The possible form of conservation laws gets a little clouded when an integral term is included as in (4). Since a convolution integral is allowed in the equation, should convolution integrals and other functionals be allowed in the conserved quantities? Presumably they have to be. This question can be by-passed for the case of (29) which we studied numerically, but at present we do not know whether it has an infinite number of conservation laws or not. Our view is that the interactions we have computed are clean, and that it is a sufficiently complicated case to make exact solutions etc. unlikely.

The other main interest in this problem is whether, in addition to the peaking of the solitary wave at the crest, the forward breaking typical of shallow water theory is also possible. To study this, we took as initial disturbance a roughly triangular shape with height 0.48 and width 1.6. The slopes of the sides are 0.6, and this is much steeper than the maximum value of 0.17 in the corresponding solitary wave of the same height. The height is considerably less than the value of 8/9 for the highest solitary wave; and the slope is less than the value $\frac{2}{9}\pi \simeq 0.7$ for that wave. The results are shown in figure 14. The forward face near the top steepens and eventually breaks. The observed velocity of the crest is approximately 0.75. This fits well with the nonlinear velocity

$3u/2$, which is 0.72 for the maximum value $u = 0.48$. It supports the view that the breaking is the usual one associated with the operator

$$u_t + \tfrac{3}{2}uu_x,$$

but the whole picture is much more complicated. The breaking seemed to depend on the forward face being steeper than the maximum for the corresponding solitary wave. Seliger (1968) had found a sufficient condition based on an initial asymmetry of the wave, with the forward slope greater than the rear slope. We saw no evidence that this was involved; however, it was known to be a very loose sufficient condition, far from necessary.

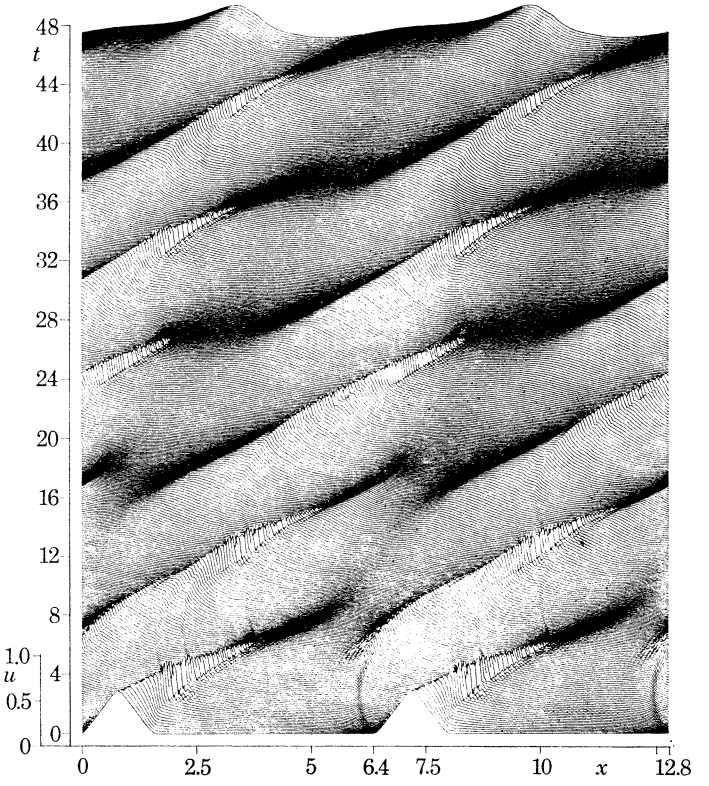

FIGURE 14. Wave breaking for integral equation
$u_t + \frac{3}{2}uu_x + \int K(x-\xi)u_\xi \,\mathrm{d}\xi = \epsilon u_{xx}, \quad K(x) = \frac{1}{2}\nu e^{-\nu|x|}, \quad \nu = \frac{1}{2}\pi, \quad \epsilon \ll 1.$

In order to continue the calculation beyond breaking a small dissipation term ϵu_{xx} was added to the equation, so that the breaking part could be replaced by a thin transition layer. In reality there remains a little jagged appearance to the breaking region, but the overall behaviour seems to be given correctly. In this case it should be remembered that the calculation is made with conditions periodic in x. We show two periods in figure 14; the latter waves include those from repetition of the initial conditions into the other periodic intervals.

The overall pattern in figure 14 appears to be that the main wave dies out as a similar one is formed at a displaced position ahead, the behaviour being reminiscent of the forward displacement of the stronger wave in soliton interactions. The breaking is superposed on this, but is not responsible for it. It would be interesting to check this for non-breaking waves. The small curved wavelets seen emanating from behind the breaking crests follow approximately a locus that fits

with the idea that they are riding on the main disturbance with velocity $3u/2$; they have fairly high wavenumbers so have little contribution from the phase speed (27) of the integral term. As u increases they curve around and merge into the next main wave also travelling with speed $3u/2$. These interpretations are tentative, however, and considerably more numerical work would be needed to understand the details fully.

7. Steps and wells

The interaction of solitary waves has naturally drawn a lot of attention, but there are many other important problems. One basic one is to find the disturbance produced by an initial step. Such a solution is often useful as a building block and provides useful insight. In gas dynamics a compressive step would produce a shock wave. In the dispersive problems considered here, the equations are reversible, there is no dissipation and the solution must have quite a different character. In the setting of plasma dynamics these solutions are often referred to as 'collisionless shocks'. In water waves they may have relevance to smooth non-turbulent bores, although even in the absence of turbulent breaking, friction still seems to play an important rôle.

For the Korteweg–de Vries equation, the problem of a step can still be formulated via inverse scattering in terms of a Marcenko integral equation, but the solution has not yet been found (to our knowledge). However, results of the earlier modulation approach (Whitham 1965, 1974) have been used by Gurevich & Pitaevskii (1974) to give the main features of the solution. The modulation approach was developed for the oscillatory solutions which are typical of dispersive problems when individual solitary waves are not involved. The local shape of the oscillations is known and equations for the local amplitude $a(x,t)$, local wavenumber $k(x,t)$, and mean level of disturbance $\bar{u}(x,t)$ can be derived. For the K. de V. equation these are hyperbolic and the solution for a step is a centred simple wave in which two of the Riemann invariants are constant everywhere, and a, k, $\bar{u}$ are functions of x/t alone.

For an initial step that increases the level we take the normalized values

$$u(x,0) = \begin{cases} -1, & x > 0, \\ 0, & x < 0, \end{cases}$$

The oscillatory disturbance is confined to

$$-2 < x/t < -\tfrac{1}{3}, \tag{32}$$

and in this range the solution is given by

$$a = s^2, \quad k = \frac{\pi}{6\tfrac{1}{2}K(s)}, \quad \bar{u} = 2\frac{E(s)}{K(s)} - 2 + s^2, \tag{33}$$

where K and E are the complete elliptic integrals and the modulus s is the function of x/t determined by

$$\frac{2-s^2}{3} + \frac{2}{3}\frac{s^2(1-s^2)\,K(s)}{E(s)-(1-s^2)\,K(s)} = -\frac{x}{t}, \quad -2 < \frac{x}{t} < -\frac{1}{3}. \tag{34}$$

These quantities are shown in figure 15 and the detailed solution constructed from them is shown in figure 16. Near the front of the wave ($x = -\frac{1}{3}t$), $s \to 1$ and the first oscillations are close to successive solitary waves. Near the back ($x = -2t$), $s \to 0$ and the solution is nearly linear.

This problem was solved numerically, from the K. de V. equation, and the results are shown in figures 17 and 18. The roughly linear increase in amplitude and smoothed step appearance of $\bar{u}$

are well represented. In figures 17 and 18, the initial step was of magnitude 10 instead of 1 so the above theoretical results have to be scaled accordingly. In particular, the velocities of the front and back of the wave become -20 and $-10/3$; the corresponding slopes have been marked in figure 18. It should be noted that these are group velocities. Towards the back of the wave where linearized theory applies, the dispersion relation is $\omega = -k^3$ and the group velocity is $-3k^2$.

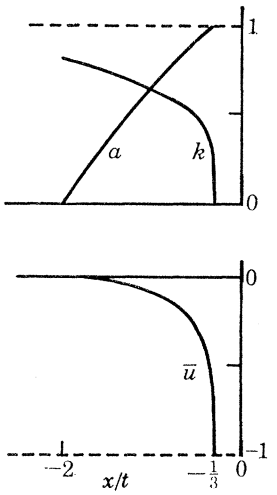

FIGURE 15

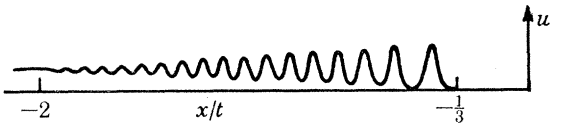

FIGURE 16

FIGURE 15. Amplitude, a, wavenumber, k, and mean height, $\bar{u}$, for positive step solution.

FIGURE 16. Detailed form of positive step solution.

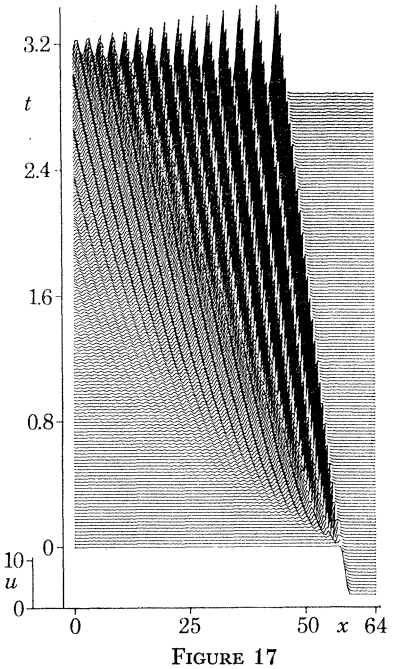

FIGURE 17

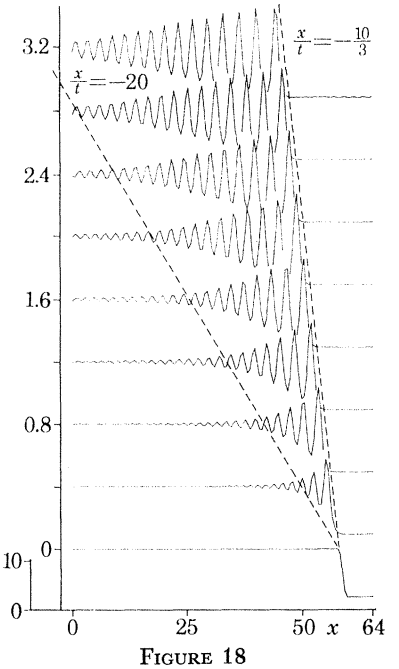

FIGURE 18

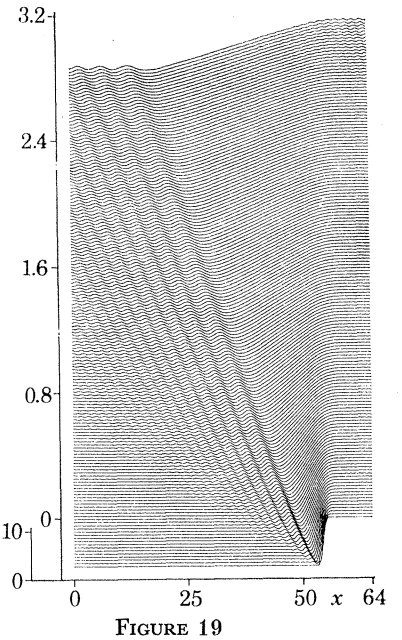

FIGURE 19

FIGURE 17. Numerical calculation of positive step solution.

FIGURE 18. Numerical calculation of positive step solution; range of modulation theory indicated by broken lines.

FIGURE 19. Numerical calculation of negative step.

According to general theory individual values of k propagate with the corresponding group velocity and we have

$$x \simeq -3k^2t, \quad k \simeq [x/(-3t)]^{\frac{1}{2}},$$

in this region. Individual crests, however, travel with the phase velocity

$$\omega/k = -k^2 \simeq x/3t.$$

Therefore, they follow paths $x \propto -t^{\frac{1}{3}}$.

These curves are easily seen in figure 17.

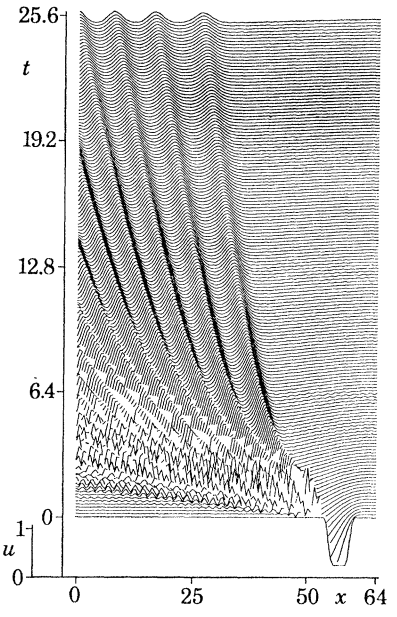

FIGURE 20

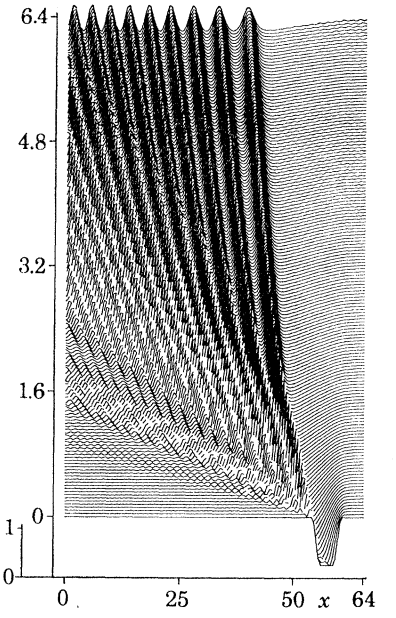

FIGURE 21

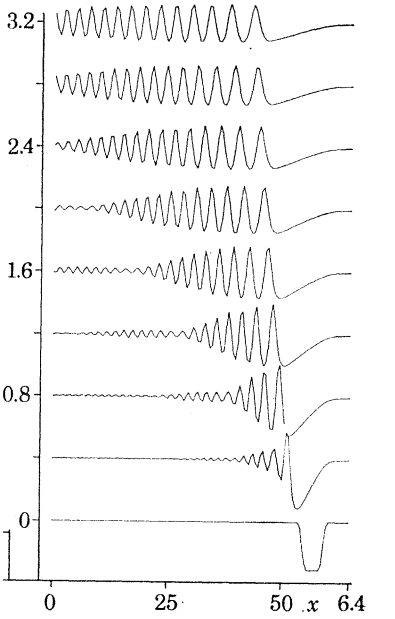

FIGURE 22

FIGURE 20. Numerical calculation for initial well.
FIGURE 21. Numerical calculation for initial well.
FIGURE 22. Numerical calculation for initial well.

When the initial step decreases the height, we take the normalized form

$$u(x, 0) = \begin{cases} 0, & x > 0, \\ -1, & x < 0, \end{cases}$$

initially. In the approximate theory, the solution is simply

$$\bar{u} = x/t, \quad -1 < x/t < 0 \tag{35}$$

and $a = 0$; there are no oscillations. This is just the appropriate solution of

$$\bar{u}_t + \bar{u}\bar{u}_x = 0 \tag{36}$$

neglecting the u_{xxx} term. The numerical calculation confirms this result as shown in figure 19. There is a small oscillation which is missed by the simple theory and is related to smoothing out the discontinuous derivative at $x/t = -1$.

The solution for an initial well combines the two step solutions. It consists of a linear profile as in figure 19 followed by an oscillatory disturbance of the type shown in figure 17. As the two parts interact the triangular shaped wave at the head stretches in length and decays in amplitude. The detailed numerical results are shown in figures 20–22.

In gas dynamics and similar dissipative systems, the triangular wave is a familiar solution. In those cases the discontinuity at the rear is a shock wave and there is no oscillatory tail. In suitable normalized form, the approximate solution satisfies (36) and is given by

$$u = \begin{cases} x/t, & -s(t) < x < 0, \\ 0, & \text{otherwise}, \end{cases}$$

where $x = -s(t)$ is the shock position. The determination of $s(t)$ depends on the choice of the correct shock condition. It leads typically to the condition:

$$\text{velocity} = \tfrac{1}{2} \times \text{strength}$$

i.e.
$$\dot{s} = \frac{1}{2}\frac{s}{t}, \quad s = Ct^{\frac{1}{2}}, \quad \text{strength} = Ct^{-\frac{1}{2}}. \tag{37}$$

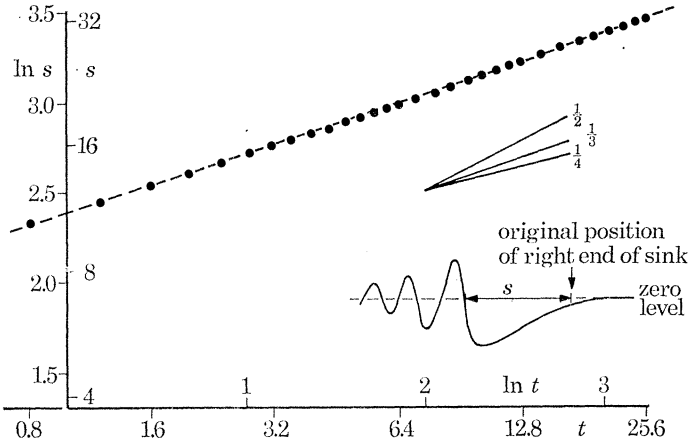

FIGURE 23. Numerical results for width s, as a function of t. The dotted background line has slope exactly $\frac{1}{3}$. The slopes corresponding to different exponents are shown above.

Since the triangular wave has width $Ct^{\frac{1}{2}}$ and depth $Ct^{-\frac{1}{2}}$, it is immediately seen that this corresponds to constant area, i.e.

$$\int_{-\infty}^{\infty} u \, dx = \text{constant}. \tag{38}$$

In gas dynamics u is proportional to the density and this choice of shock condition is equivalent to conservation of mass.

In the dispersive case, we might try to view the result as a triangular wave for the mean level $\bar{u}$, with the oscillatory tail superposed to carry energy away in place of dissipation. Then we have a simple approach that would perhaps be helpful in other more complicated problems. A key question would be the correct choice of 'shock' condition. Conservation of mass (or volume) with the results in (37) would still be a candidate. However, it is possible that mass as well as energy is transferred under the oscillatory tail. An alternative is suggested by the simple step solution. According to (34) the front in that case propagates according to $x/t = -\frac{1}{3}$, i.e. the velocity is $\frac{1}{3}$ of the strength. This condition would give

$$\dot{s} = \tfrac{1}{3}s/t, \quad s = Ct^{\frac{1}{3}}, \quad \text{strength} = Ct^{-\frac{2}{3}}, \tag{39}$$

in the more general context. It is intersting that this choice corresponds to the conservation of

$$\int_{-\infty}^{\infty} |\bar{u}|^{\frac{1}{2}} \, \mathrm{d}x,$$

because this quantity is also important in various ways in the discussion of solitary waves (Whitham 1974, §17.5).

From the numerical results, it is possible to get a very clear plot of s, and the exponent $\frac{1}{3}$ is quite definitely indicated (see figure 23). The exponent $\frac{1}{3}$ is also found in the theoretical discussion of Ablowitz & Segur (1977).

8. Wavetrain instabilities

Periodic wavetrains are basic solutions in dispersive problems. Among other things, they are used to develop the modulation theory referred to in the last section. In the nonlinear case, they may be unstable to small disturbances. One way to see this is from the modulation theory itself. For the simplest problems, (when there is no coupling of the oscillatory disturbance with various mean levels such as the $\bar{u}$ of the last section), the modulation equations for the local amplitude $a(x,t)$ and local wavenumber $k(x,t)$ are approximately

$$k_t + \omega_x = 0,$$

$$(a^2)_t + (\omega_0' a^2)_x = 0,$$

$$\omega = \omega_0(k) + \omega_2(k)\, a^2 - \tfrac{1}{2}\omega_0''(k)\, a_{xx}/a;$$

$\omega_0(k)$ is the linear dispersion relation and $\omega_2(k)$ is the coefficient of the linear correction. For the uniform wavetrain, a and k are constant, and it is easily shown that perturbed solutions in the form

$$\delta a, \delta k \propto \mathrm{e}^{\mathrm{i}\mu(x-Vt)}$$

have

$$V = \omega_0' \pm (\omega_0''\omega_2 a^2 + \tfrac{1}{4}\omega_0''^2\mu^2)^{\frac{1}{2}}.$$

If $\omega_0''\omega_2 > 0$, the values of V are real and give nonlinear generalizations of the linear group velocity ω_0'. If $\omega_0''\omega_2 < 0$, small modulations will grow for values of μ in the range

$$0 < \mu^2 < 4|\omega_2/\omega_0''|\, a^2.$$

The growth rate depends on

$$\mu(|\omega_0''\omega_2|\, a^2 - \tfrac{1}{4}\omega_0''^2\mu^2)^{\frac{1}{2}}, \tag{40}$$

and is a maximum for

$$\mu^2 = 2|\omega_2/\omega_0''|\, a^2. \tag{41}$$

One of the earliest and most interesting instances of this instability is again in water wave theory. For waves on deep water

$$\omega_0 = (gk)^{\frac{1}{2}}, \quad \omega_2 = \tfrac{1}{2}k^2(gk)^{\frac{1}{2}},$$

so we have $\omega_0''\omega_2 < 0$. The analysis has to be extended for finite depth. For the Korteweg–de Vries equation, for example, the additional variable $\bar{u}$ appears in the modulation equations and the wavetrains are stable.

In order to study this situation and the further development of disturbances numerically we chose one of the simpler examples where the instability is found, and the equation

$$u_t + 3u^2u_x + u_{xxx} = 0 \tag{42}$$

is such a case. For it has

$$\omega_0 = -k^3, \quad \omega_2 = \tfrac{3}{4}k, \quad \omega_0''\omega_2 < 0.$$

The growth rate in (40) is $$3k\mu(\tfrac{1}{2}a^2-\mu^2)^{\frac{1}{2}}, \tag{43}$$

with a maximum for $$\mu = \tfrac{1}{2}a.$$

The computations were first run with the known exact periodic wavetrain solution as initial condition. Since it should just translate with constant velocity and without change in form, the idea was that this would check out the method. Results of the type shown in figure 24 were found. Small numerical errors triggered the instability automatically, and there was no need to add them explicitly in the initial data. It should be stressed that it is not that numerical errors grow, but that they act as perfectly good initial perturbations.

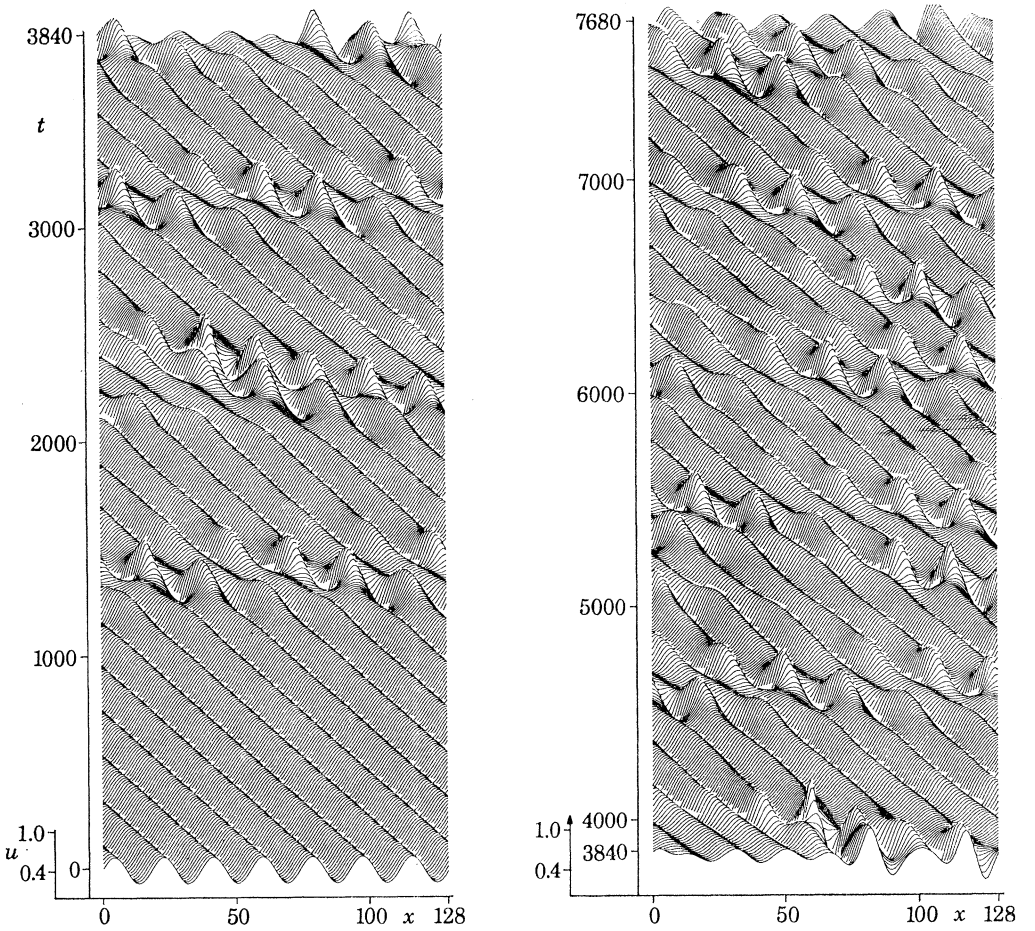

FIGURE 24. Instabilities of nonlinear wavetrain.

We were surprised not so much by the complete returns to the uniform wavetrain (which may be similar to the periodicity found by Zabusky & Kruskal (1965) for the Korteweg–de Vries equation), but by the long intervals between the earlier bursts, and the persistence of returns for the very long times shown in figure 24. However, it is true that approximate theories involving the interaction of a finite number of Fourier modes predict this. For the finite system, initially small modes grow taking energy from the others, but eventually they in turn lose energy to the others and die away again. The energy in the system, which is conserved, oscillates between the modes. An appropriate version of this type of theory is used to interpret our results.

It starts from a study sideband interactions, following Benjamin's original analysis of the instability of deep water waves. We note some of the details for (42). Solutions of the form $u = \frac{1}{2}A_0(t)\,e^{ikx} + \frac{1}{2}A_1(t)\,e^{i(k-\mu)x} + \frac{1}{2}A_2(t)\,e^{i(k+\mu)x}$ + complex conjugates are considered, where the sidebands A_1 and A_2 are initially small. In the nonlinear interactions, various products feed back on the original components. For example, triple products with exponents

$$k+\mu, \quad k-\mu, \quad -k$$

produce a contribution to the term e^{ikx}. When these resonating third order interactions are included but all others are neglected, and the generation of modes such as $k \pm 2\mu$ is neglected, we have

$$(i/k)\,dA_0/dt + k^2A_0 = \{\tfrac{3}{4}A_0A_0^* + \tfrac{3}{2}A_1A_1^* + \tfrac{3}{2}A_2A_2^*\}A_0 + \tfrac{3}{2}A_1A_2A_0^*, \tag{44}$$

$$[i/(k-\mu)]\,dA_1/dt + (k-\mu)^2A_1 = \{\tfrac{3}{2}A_0A_0^* + \tfrac{3}{4}A_1A_1^* + \tfrac{3}{2}A_2A_2^*\}A_1 + \tfrac{3}{4}A_0^2A_2, \tag{45}$$

and a similar equation for A_2. The first terms on the right represent self-interaction and the effect of each wave riding on the others. It is the last term that produces the energy transfer.

If these equations are linearized on the basis that $A_1, A_2 \ll A_0$, the previous instability result (43) is recovered with the sideband interpretation for μ. But we can take the analysis further without making the linearized approximation (Benney 1962; Bretherton 1964). The key to this is that three integrals of the equations can be found:

$$\frac{|A_0|^2}{k} + \frac{|A_1|^2}{k-\mu} + \frac{|A_2|^2}{k+\mu} = \text{constant}, \tag{46}$$

$$|A_0|^2 + |A_1|^2 + |A_2|^2 = \text{constant}, \tag{47}$$

$$A_0^2A_1^*A_2^* + A_0^{*2}A_1A_2 - \tfrac{4}{3}\{k^2|A_0|^2 + (k+\mu)^2|A_1|^2 + (k-\mu)^2|A_2|^2\}$$
$$+ 2\{|A_0|^2|A_1|^2 + |A_0|^2|A_2|^2 + |A_1|^2|A_2|^2\} + \tfrac{1}{2}\{|A_0|^4 + |A_1|^4 + |A_2|^4\} = \text{constant}. \tag{48}$$

These can be derived by applying Noether's theorem to the invariances of the corresponding variational principle. The more forbidding one, (48), is in fact the simplest and comes from the invariance in time; the others follow from invariance to phase changes in the complex amplitudes A_n. (These and other details are noted in appendix A.) When the integrals are used, a single equation for $|A_1|^2$, say, can be obtained, and it has solutions in terms of elliptic functions. In the limiting case when the modulus tends to 1, the period tends to infinity and we have a single swing given by

$$\frac{|A_1|^2}{k-\mu} = \frac{|A_2|^2}{k+\mu} = \frac{a^2 - |A_0|^2}{2k} \tag{49}$$

$$= \frac{16\mu^2(a^2-2\mu^2)/k}{(12\mu^2+a^2) + (16\mu^2-a^2)\cosh 6k\mu\,(\frac{1}{2}a^2-\mu^2)^{\frac{1}{2}}t}. \tag{50}$$

This shows the growth of the side bands in accordance with (43), but a maximum is reached and the side bands decay again.

For the side bands of maximum growth rate we have $\mu = \frac{1}{2}a$ and the maximum value in (50) gives

$$|A_0|^2 = \tfrac{3}{7}a^2, \quad |A_1|^2 = \left(1-\frac{\mu}{k}\right)\tfrac{2}{7}a^2, \quad |A_2|^2 = \left(1+\frac{\mu}{k}\right)\tfrac{2}{7}a^2. \tag{51}$$

The time scale, estimated as the time taken from 10 % of maximum to the maximum is

$$T = 2.5/ka^2. \tag{52}$$

To see whether this solution could be used to interpret the bursts seen in the computations, the amplitudes of the individual harmonics in the numerical results were noted. Since the problem was formulated to be periodic over a large space interval and the Fourier method used, these were readily available. Results are shown in figure 25. The wavenumbers present are integer multiples of a basic unit which in the cases shown is $\frac{1}{64}\pi$. In figure 25 the initial wavetrain has $a = 0.2$, $k = 7$ units. The initial function in this run was actually $0.2 \sin(\frac{7}{64}\pi x)$ with no higher harmonics present. This is why in figure 25*a* we can see a fast oscillation between mode 7 and the first higher harmonic, mode 21.

As other test runs show (with precise uniform wavetrains as initial function) this oscillation does not in any noticeable way influence the wavetrain instabilities we are studying, not even

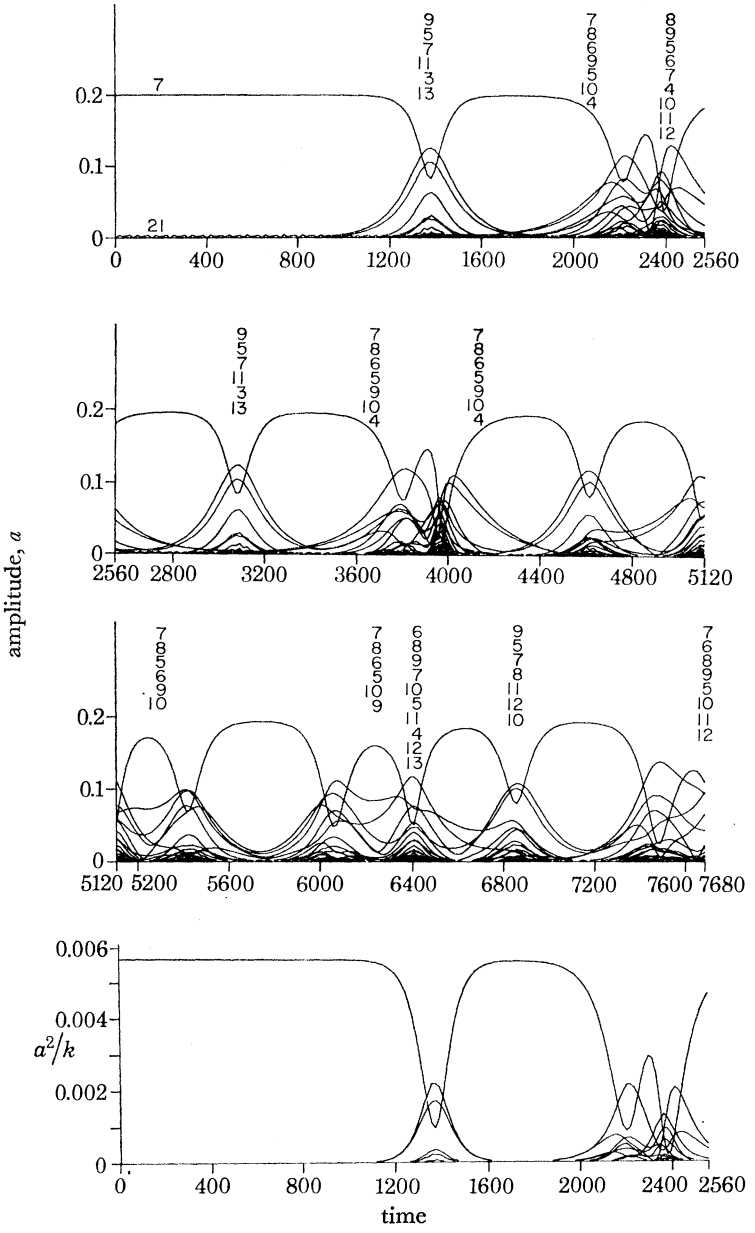

Figure 25*a*

Figure 25*b*

Figure 25*c*

Figure 25*d*

FIGURE 25. Amplitudes of harmonics in wavetrain instabilities.

how quickly they are triggered. According to (43) the most rapidly growing sidebands have $\mu = 0.1 \simeq 2$ units. The wavenumbers present are indicated by the integers over the maximum points in the interaction, in the same order top to bottom as the curves. The two sidebands $k-\mu = 5$ and $k+\mu = 9$ are the dominant ones as the simple theory would indicate. However modes with wavenumbers $k \pm m\mu$ are also generated; this is because, for example, products with wavenumbers

$$k+\mu, \quad k+\mu, \quad -k$$

generate $k+2\mu$, and so on. Although these are not included in the theory (the case of 5 interacting modes seemed to defy much progress) we can check the general order of magnitude from (51). These would give

$$|A_0| = 0.13, \quad |A_1| = 0.09, \quad |A_2| = 0.12.$$

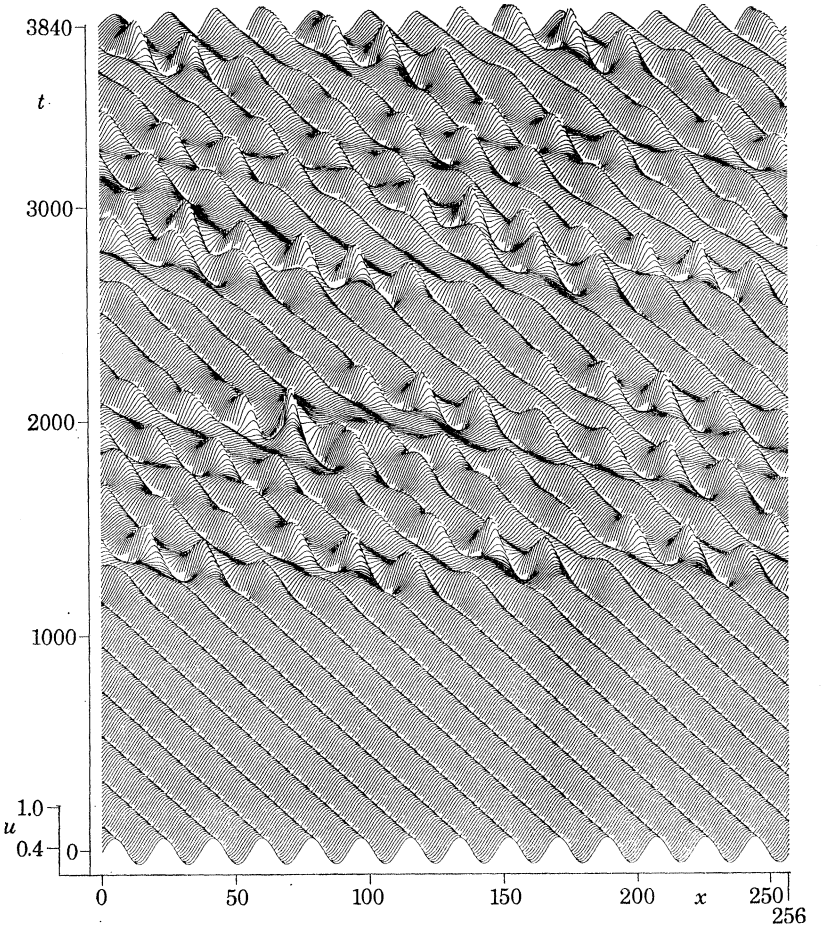

FIGURE 26. Instabilities of nonlinear wavetrain.

This is taken to be good agreement; the extra drain on $|A_0|$ is interpreted as being due to the extra drain of the additional sidebands. The time scale given by (52) is $T = 180$ which is also reasonable. The plots of (amplitude)^2/wavenumber, which are significant quantities in the solution (50) are shown in figure 25*d*. This quantity is the same for sidebands 9 and 5, in agreement with (49), until the other sidebands intrude and upset the balance. The second burst in figure 25*a* appears to be triggered by sidebands 6 and 8 ($\mu = 1$), which are also unstable but take longer to grow, and then

they tangle with the recurrence of 5 and 9. For the longer times shown in figures 25*b* and *c*, there is more activity in the bursts and increasingly more between the main bursts.

Three cases of sideband instabilities were studied numerically. Apart from the case $k = \frac{7}{64}\pi$, $a = 0.2$ as in figures 24 and 25, we also computed $k = \frac{10}{64}\pi$, $a = 0.2$ and $k = \frac{10}{64}\pi$, $a = 0.3$. The times from the starts of the runs to the middles of the first burst were $t = 1360$, $t = 925$ and $t = 415$ respectively. These also agree very well with a time scale of the form $T = \text{const}/ka^2$.

When the basic interval is doubled, so that the wavenumber unit is reduced to $\pi/128$, there are more sidebands in the unstable range and more activity. Results are shown in figure 26, where it is clear that the bursts last longer, are more complicated and there is only one short return to the original wavetrain. As the interval is increased further we expect continuous activity after the first burst.

9. Accuracy of the numerical scheme

The usual way to analyse the accuracy of a numerical scheme is to study the local truncation error as a function of the mesh spacing. In particular for linear equations, this allows an estimate of total accumulated errors during a time integration. In the present context, such a study would be inadequate for several reasons:

(*a*) Almost all effects we study are due to nonlinear processes. A pseudospectral method (or any method using Fourier space representation) could depend unusually heavily on the linear nature of an equation.

(*b*) Even for linear equations, the accuracy of a pseudospectral method for a non-smooth solution is not due to small truncation errors but to cancellations of rather large but oscillatory truncation errors during the time integration.

We would like to have a method of analysis which circumvents these problems, in particular the point in (*b*), while still using a test which is local in time (i.e. does not involve actual numerical time integration).

The instabilities of uniform wavetrains offer a good possibility for such a study of nonlinear accuracy at least for one particular case of strictly nonlinear effects. In the previous section we analysed wavetrain instabilities by inserting a main mode and two symmetric sidebands into (42). The interchanges between these modes were described in equations (49) and (50). The solution could be followed in time all the way through the instability.

An alternative version is described by Driscoll & O'Neil (1976). We look for any small perturbations v_0 of the main wave u_0, which grow locally exponentially in time. In this way we can only describe the very beginning of the development of the instability. On the other hand, no assumption is made about the form of the unstable perturbation. Let us consider the specific case of a uniform wavetrain for the equation

$$u_t + 3u^2u_x + u_{xxx} = 0, \quad x\text{-interval } 0 \quad \text{to} \quad 128, \tag{53}$$

with main component of $u(x,t)$ given by $u(x,t) = 0.3\cos\nu(x-ct), \nu = (7\times 2\pi)/128$ (seven oscillations within the interval). An approximation of a wavetrain with this leading mode may be found by substitution into (53):

$$\begin{aligned} u_0(x-ct) &= 0.3\cos\nu(x-ct) + 0.00769624\cos 3\nu(x-ct) \\ &\quad + 0.00019263\cos 5\nu(x-ct) \\ &\quad + 0.00000482\cos 7\nu(x-ct) + 0.00000012\cos 9\nu(x-ct) + \ldots \\ c &= -0.04874619. \end{aligned} \tag{54}$$

In the following, we simplify the problem somewhat by transforming to a frame of reference moving with speed c. Equation (53) becomes

$$u_t + (3u^2 - c)\, u_x + u_{xxx} = 0 \tag{55}$$

and the wavetrain in (55) is now stationary. We substitute $u(x,t) = u_0(x) + \mathrm{e}^{\alpha t} v_0(x)$ into (55). Assuming $u_0(x)$ is a time independent solution of (55) and ignoring second order quantities in v_0 we get

$$\alpha v_0 - c v_{0x} + 3u_0^2 v_{0x} + 6u_0 v_0 u_{0x} + v_{0xxx} = 0 \tag{56}$$

$$\alpha v_0 - c v_{0x} + 3(u_0^2 v_0)_x + v_{0xxx} = 0. \tag{57}$$

We can transform (57) to Fourier space and, keeping only a finite number of modes, solve the equation as a linear eigenvalue problem for matrices. The eigenvalues are α with eigenvectors v_0. The unstable perturbations appear as eigenvectors corresponding to eigenvalues with non-zero real parts. When we increase the number of modes, the eigenvalues α converge rapidly to the numbers given in table 2. We denote here the main mode as mode 7 and note for each unstable solution its dominant sidebands. These four solutions are the only unstable ones.

TABLE 2

dominant sidebands	growth rate, α
6, 8	0.0101916188
5, 9	0.0184643383
4, 10	0.0220767943
3, 11	0.0130214545

These results also allow a check on the approximate formula in (43). For $a = 0.3$, $k = \frac{7}{64}\pi$, $\mu = \frac{1}{64} m\pi$, the growth rate would be

$$0.002484\, \mathrm{m}\, \{18.68 - m^2\}^{\frac{1}{2}}.$$

This would predict instability for sidebands with $m = 1, 2, 3, 4$ and the corresponding growth rates would be

$$0.01044, \quad 0.01903, \quad 0.02318, \quad 0.01625,$$

respectively. These are quite good approximations to the values in table 2.

If the space derivatives of (55) are approximated by certain finite difference approximations, the corresponding unstable modes may be studied by using the same difference approximations in (56) (but not in (57)). Equation (56) becomes a discrete linear eigenvalue problem.

We restrict this study to discretization in space only (the analysis can be done as well for finite time steps). This means that it will not reflect the difference between the methods represented by (9) and (10). For difference approximations of finite width the matrices will have a cyclic band structure. The equivalent difference formula to the proposed scheme covers the full interval and the matrix is a full matrix.

For compact 2nd to 8th order difference approximations to the spatial derivatives the eigenvalues in our example were calculated for number of mesh points $n = 2^k$, $k = 6, 7, \ldots, 11$. These large eigenvalue problems could, because of their structure, be handled efficiently by Newton's method as described by Peters & Wilkinson (1978). For the full matrices generated by the

proposed scheme, routines from EISPACK (Smith *et al.* 1974) were used with values of n ranging from 64 to 160.

The growth rates in the numerical schemes were compared against the values in table 2 and the relative errors were calculated. The logarithm (base 10) of the largest of these errors for any of the four modes is plotted in figure 27 for all cases that were tested.

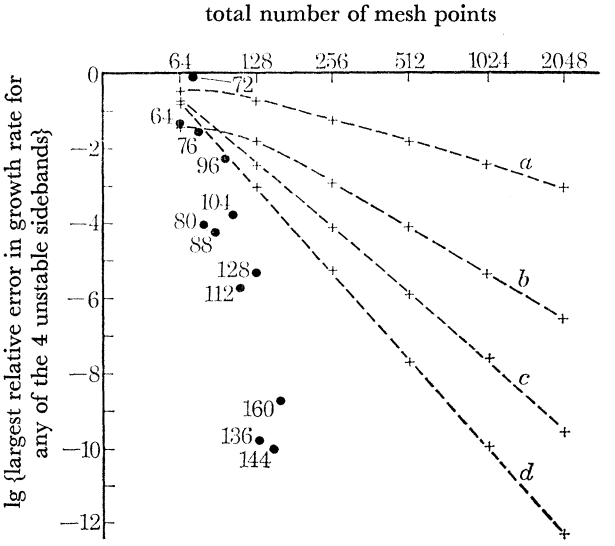

FIGURE 27. Comparison of nonlinear accuracies in numerical schemes. Curve (*a*) 2nd order method, (*b*) 4th order method, (*c*) 6th order method, (*d*) 8th order method. ●, proposed method.

The curves in figure 27 for the 2nd to 8th order methods are smooth but for the proposed scheme rather irregular. This irregularity should be expected since the scheme attempts an exact treatment of all modes present. For n increasing, high harmonics of the dominant mode 7 suddenly appear in the range that is correctly treated instead of being either lost or incorrectly fed back on top of a sideband.

Figure 27 shows that the advantage of high order methods, well known for linear problems, is at least as pronounced for this strongly nonlinear problem. To achieve the same accuracy as the proposed scheme for 128 points (the resolution we used in most of the numerical calculations) a second order scheme would need about 10000 points. Already in one space dimension and for implicit schemes without a stability condition $\Delta t/\Delta x^3 <$ constant, a method of such low order seems to compare unfavourably. Difference schemes of higher orders are much more attractive. Implicit high order methods have however the drawback that the operation count per time step increases quadratically with the order and not linearly as for explicit schemes.

This research was supported by the Office of Naval Research, U.S. Navy and by E.R.D.A. (Grant 04-3-767).

Appendix A. Discussion of equations (44)–(45)

These equations follow from a variational principle with Lagrangian

$$L = \sum_n \left\{ \frac{\mathrm{i}}{2k_n} \left(A_n^* \frac{\mathrm{d}A_n}{\mathrm{d}t} - A_n \frac{\mathrm{d}A_n^*}{\mathrm{d}t} \right) + k_n^2 |A_n|^2 - \tfrac{3}{8} |A_n|^4 \right\} - \tfrac{3}{2} \sum_{m<n} |A_m|^2 |A_n|^2 - \tfrac{3}{4} \{ A_0^2 A_1^* A_2^* + A_0^{*2} A_1 A_2 \}, \tag{A 1}$$

where summation is over $n = 0, 1, 2$, and

$$k_0 = k, \quad k_1 = k + \mu, \quad k_2 = k - \mu. \tag{A 2}$$

This can be seen directly or derived from the variational principle

$$\delta \int\int (-2\phi_x \phi_t + 2\phi_{xx}^2 - \phi_x^4) \, \mathrm{d}x \, \mathrm{d}t = 0 \tag{A 3}$$

for the modified K. de V. equation (42) with $u = \phi_x$ and

$$\phi = -\sum_n \frac{\mathrm{i}}{2k_n} A_n \, \mathrm{e}^{\mathrm{i}k_n k} + \text{c.c.} \tag{A 4}$$

When the Lagrangian is invariant to translations in time, Noether's theorem gives the integral

$$\sum_j (\dot{A}_j L_{\dot{A}_j} + \dot{A}^* L_{\dot{A}_j^*} - L) = \text{const.}$$

Applied to (A 1), this leads immediately to (48).

The other obvious invariances in (A 1) are changes in phase

$$A_n \to A_n \, \mathrm{e}^{\mathrm{i}\epsilon_n},$$

with

$$2\epsilon_0 - \epsilon_1 - \epsilon_2 = 0.$$

The corresponding integral according to Noether's theorem is

$$\sum_j (\mathrm{i}\epsilon_j A_j L_{\dot{A}_j} - \mathrm{i}\epsilon_j A_j^* L_{\dot{A}_j^*}) = \text{const.}$$

This leads to two independent invariants; with $\epsilon_1 = \epsilon_2 = \epsilon_0$ we obtain (46), with $\epsilon_n = k_n$ we have (47).

The remaining major step in simplifying the equations for the A_n is to note that the symmetric terms on the right of (44) can be eliminated by multiplying it by A_0^* and taking the difference of the resulting equation from its conjugate. This gives

$$A_0^2 A_1^* A_2^* - A_0^{*2} A_1 A_2 = -\frac{2\mathrm{i}}{k} \frac{\mathrm{d}}{\mathrm{d}t} |A_0|^2. \tag{A 5}$$

We then note that (48) may be used to express the related quantity

$$A_0^2 A_1^* A_2^* + A_0^{*2} A_1 A_2 = F \tag{A 6}$$

as a function of $|A_0|^2$, $|A_1|^2$, $|A_2|^2$ alone.

If we square these and take the difference, we have

$$\frac{4}{k^2} \left(\frac{\mathrm{d}|A_0|^2}{\mathrm{d}t} \right)^2 = 4|A_0|^4 |A_1|^2 |A_2|^2 - F^2. \tag{A 7}$$

From (46) and (47), $|A_1|^2$ and $|A_2|^2$ may be expressed in terms of $|A_0|^2$; the right hand side is then a quartic in $|A_0|^2$ and solutions may be obtained in elliptic functions. A limiting case is the solution quoted in (49).

Appendix B. Instabilities of the proposed scheme

One well known feature of leap-frog time differencing is the possibility of separation of the solution between two successive time levels. There is no way for the leap-frog scheme to detect if every second time level has a constant value added to it. If the solution is accurate, this separation should not occur (since every level approximates a unique solution). In the present calculations, no separation occurred for soliton interactions. The effect appeared however in the calculations of the unstable wavetrains. This could be expected since small roundoff errors, uncorrelated for odd and even time steps, triggered large scale effects for unstable solutions. This possibility of separation has sometimes been considered a major weakness (see Gazdag 1976 for references) making leap-frog not a competitive method. The problem is however easily circumvented. When we have calculated the solution up to levels $t-\Delta t$, t, and $t+\Delta t$, we can introduce levels $t-\frac{1}{2}\Delta t$, and $t+\frac{1}{2}\Delta t$ as averages of adjacent levels and restart the scheme from these two new levels. This process was repeated every 40 time steps in the calculation of the unstable wavetrains.

The commonly suggested alternative would be to use an Adams–Bashforth type scheme or to use leap-frog only as a predictor together with a corrector linking the latest two time levels to each other. It is not obvious how to implement this in a stable way based on analytic solution of the linear part.

Another possibility of separation in leap-frog type schemes is that every second mesh value for fixed t may separate from every other second value. For the simplest approximation of $\partial u/\partial t + \partial u/\partial x = 0$ with centred differences in both space and time, the separation is complete and the scheme falls apart in two separate schemes, each on its own grid. In our case there is no complete separation, but frequency component 65 (which corresponds to the separation of every second point on a grid with 128 points) behaved in a few cases slightly irregularly. It was cut out of every 40 time steps, every 80 time steps components 61–65 were cut out. This control of possible decoupling of the scheme should not be interpreted as smoothing to supress nonlinear instabilities.

It was shown by Fornberg (1973) that nonlinear instabilities for $u_t + uu_x = 0$, approximated by a leap-frog scheme, can be expected only where u is close to zero. This is at places where small irregularities in the solution are stationary relative to the mesh. Nonlinear instabilities observed in the present calculations follow the same pattern. No instabilities were observed when the linear part was $u_t + u_{xxx} = 0$. Small irregularities contain high frequency components and are never stationary. With the integral kernel $K(x) = \frac{1}{2}\nu e^{-\nu|x|}$ in (4) very high frequency components are translated only by the nonlinear term. In very few cases, nonlinear instabilities were now observed, but they could always be avoided by introducing a translation with an extra u_x-term, i.e. without any dissipation. The soliton interactions in figure 13 were actually calculated from the equation

$$u_t + \tfrac{3}{2}uu_x + \int K(x-\xi)\, u_\xi \,\mathrm{d}\xi = 0 \qquad \text{(B 1)}$$

instead of

$$u_t + \tfrac{3}{2}uu_x - \tfrac{5}{4}u_x + \int K(x-\xi)\, u_\xi \,\mathrm{d}\xi = 0.$$

In figure 13 the curves have been shifted periodically to compensate for the missing term $-\frac{5}{4}u_x$. In spite of long intervals with values around zero for (B 1), no instability showed up in this particular case.

Aliasing

Aliasing refers to the fact that very high frequency components cannot be distinguished from low ones on a discrete mesh. These high components may have been generated by nonlinear interactions and they will at later time steps be interpreted as low frequency components. Opinions about this phenomenon as a source of error are very varying, ranging from catastrophic, Schamel & Elsässer (1976), to no problem whatsoever, Fox & Orszag (1973). The experiences from the present calculations as well as from the accuracy analysis agree best with the last conclusion.

It was shown by Fornberg (1975) that the Fourier method to find derivatives is only a different way to describe the limit method of classical finite difference approximations of $\partial/\partial x$ with formal accuracies tending to infinity. The fast Fourier transform can be used to evaluate this limit efficiently. This is because the problem is equivalent to a periodic discrete convolution, and in the discrete Fourier space, these convolutions correspond to pointwise multiplications. There are other transforms, for example the 'fast number-theoretical transforms' (Agarwal & Burrus, 1975) which also support fast convolutions. Such transforms could have been used equally well to implement the proposed scheme. Fourier representation does not necessarily enter in the calculation. It is not obvious that Fourier space is the most suitable space for theoretical discussions of certain nonlinear effects. (Nonlinear instabilities for example were first attributed to aliasing (Phillips 1959) after arguments in Fourier space, but later found to have a local and well defined structure in physical space (Fornberg 1973)).

The situation may however be different if the scheme is advanced in time in the Fourier space. Then the Fourier representation enters into the calculation.

Technical data for the different runs

The details of the numerical work for the different figures are given in table 3.

TABLE 3. TECHNICAL DATA FOR THE DIFFERENT RUNS

figure	$2N$, mesh points in x-direction	Δx	Δt	total number of time steps	comment
1	128	1.0	0.025	15360	Computational period [0, 128]. Figure shows two copies of the solution side by side with one of the two sets of interactions suppressed in the picture.
2	128	1.0	0.05	2400	Centre of interaction computed with the refined grid. Not necessary for figure 2 but the two cases were run together.
3	128	0.5	0.008	25000	
4, 5, 6,	256	0.5	0.0125	25600	
7, 8, 9, 10	128	1.0	0.05	6400	
11	128	0.5	0.01	3200	
12	128	1.0	0.05	12800	
13	128	0.4	0.008	51200	
14	128	0.05	0.005	9600	Actual spatial period [0, 6.4]. Figure shows two copies of same solution side by side.
17, 18, 19	512	0.5	0.001	3200	All figures from same run. Each figure displays 128 points.
20, 21, 22	512	0.5	0.002	12800	All figures from same run. Each figure displays 128 points.
24	128	1.0	0.05	153600	
26	256	1.0	0.05	76800	

REFERENCES

Ablowitz, M. J. & Segur, H. 1977 *Stud. appl. Math.* (in the press).
Agarwal, R. C. & Burrus, C. S. 1975 *Proc. IEEE* **63**, 550–560.
Benney, D. J. 1962 *J. Fluid Mech.* **14**, 557–584.
Bretherton, F. P. 1964 *J. Fluid Mech.* **20**, 457–479.
Cooley, J. W., Lewis, P. A. W. & Welch, P. D. 1969 *IEEE Trans. Education* E-12 no. 1, 27–34.
Cooley, J. W., Lewis, P. A. W. & Welch, P. D. 1970 *J. Sound Vibr.* **12**, 315–337.
Cooley, J. W. & Tukey, J. W. 1965 *Math. Comp.* **19**, 297–301.
Dodd, R. K. & Bullough, R. K. 1976 *Proc. R. Soc. Lond.* A **351**, 499–523.
Dodd, R. K. & Bullough, R. K. 1977 *Proc. R. Soc. Lond.* A **352**, 481–503.
Driscoll, C. F. & O'Neill, T. M. 1976 *Phys. Rev. Lett.* **37**, 69–72.
Fornberg, B. 1973 *Math. Comp.* **27**, 45–57.
Fornberg, B. 1975 *SIAM J. Numer. Anal.* **12**, 509–528.
Fox, D. C. & Orszag, S. A. 1973 *J. Comp. Phys.* **11**, 612–619.
Gardner, C. S., Greene, J. M., Kruskal, M. D. & Miura, R. M. 1967 *Phys. Rev. Lett.* **19**, 1095–1097.
Gardner, C. S., Greene, J. M., Kruskal, M. D. & Muria, R. M. 1974 *Commun. Pure appl. Math.* **27**, 97–133.
Gazdag, J. 1976 *J. Comp. Phys.* **20**, 196–207.
Gurevich, A. V. & Pitaevskii, L. P. 1974 *J. exp. theor. Phys.* **38**, 291–297.
Hirota, R. 1972 *J. Phys. Soc. Japan* **33**, 1456–58.
Kreiss, H.-O. & Oliger, J. 1972 *Tellus* **24**, 199–215.
Lax, P. D. 1968 *Commun. Pure appl. Math.* **21**, 467–490.
Peters, G. & Wilkinson, J. H. 1978 (to be published).
Longuet-Higgins, M. S. 1976 *Proc. R. Soc. Lond.* A **350**, 1–26.

Phillips, N. A. 1959 *The atmosphere and sea in motion* (ed. B. Bolin), pp. 501–504. New York: Rockefeller Institute.
Schamel, H. & Elsässer, K. 1976 *J. Comp. Phys.* **22**, 501–516.
Seliger, R. L. 1968 *Proc. R. Soc. Lond.* A **303**, 493–496.
Smith, B. T., Boyle, J. M., Garbow, B. S., Ikebe, Y., Klema, V. C. & Moler, C. B. 1974 *Matrix eigensystems routines – EISPACK Guide.* Berlin: Springer-Verlag.
Tappert, F. 1974 *Lect. appl. math. Am. Math. Soc.* **15**, 215–216.
Vliegenthart, A. C. 1971 *J. Engng Math.* **5**, (2), 137–155.
Whitham, G. B. 1965 *Proc. R. Soc. Lond.* A **283**, 238–261.
Whitham, G. B. 1967 *Proc. R. Soc. Lond.* A **299**, 6–25.
Whitham, G. B. 1974 *Linear and nonlinear waves.* New York: Wiley-Interscience.
Zabusky, N. J. & Kruskal, M. D. 1965 *Phys. Rev. Lett.* **15**, 240.
Zhakarov, V. E. & Faddeev, L. D. 1972 *Funct. Analysis Applics* **5**, 280–287.
Zhakarov, V. E. & Shabat, 1972 *Sov. Phys. J. Exp. Theor. Phys.* **34**, 62–69.